Award Number: 06HQGR0202

BIAS IN NEAR FAULT GROUND MOTION RECORDINGS OF RECENT LARGE EARTHQUAKES

FINAL REPORT

November 17, 2007

P. Somerville, R. Graves and N. Collins*

URS Group, Inc.

566 El Dorado Street
Pasadena, CA 91101

Tel: (626) 449-7650
Fax: (626) 449-3536

*Email: paul_somerville@urscorp.com

Research supported by the U.S. Geological Survey (USGS), Department of the Interior, under award number 06HQGR0202. The views and conclusions contained in this document are those of the authors and should not be interpreted as necessarily representing the official policies, either expressed or implied, of the U.S. Government.

BIAS IN NEAR FAULT GROUND MOTION RECORDINGS OF RECENT LARGE EARTHQUAKES

SUMMARY

At short and intermediate periods (0.3-3.0s), the recorded ground motions from recent large crustal earthquakes, such as the Mw 7.6 1999 Chi-Chi, Taiwan, Mw 7.4 1999 Kocaeli (Izmit), Turkey and Mw 7.9 2002 Denali, Alaska earthquakes are systematically weaker than those predicted by ground motion models that are currently in use. These ground motion recordings have been combined with other strong motion data and used to produce a new set of ground motion models in the Next Generation Attenuation (NGA) Program. The NGA ground motion models are based on a much larger and better documented data set that contains many more recordings of earthquakes larger than magnitude 7, compared with the previous generation of models, summarized by Abrahamson and Shedlock (1997), which were used in the current maps.

Inclusion of these recordings in the development of the NGA models has lead to reductions by amounts ranging from 15 – 30% in the levels of ground motions predicted for large earthquakes. Moreover, for most of the NGA models, the strong motion data for the recent large earthquakes required oversaturation at short periods and close distances, that is, ground motion level decreasing with increasing magnitude above about magnitude 7. These NGA models were constrained not to oversaturate, but they do saturate at about magnitude 7, i.e. short period near fault ground motions stop increasing with magnitude above M 7.

The USGS is using the NGA models in its upcoming revision of the National Seismic Hazard Maps. However, members of the USGS hazard mapping team (Frankel and Petersen, personal communication) have expressed the concern that, for some of the sparsely recorded earthquakes, including the 2002 Denali and 1997 Kocaeli (Izmit) events, the recorded ground motions may not be representative of the median levels of ground motions caused by these earthquakes. In particular, there is concern that the tendency for oversaturation in the NGA models is a symptom of bias in the sparse strong motion recordings of these earthquakes.

The objective of this project is to use broadband ground motion simulations of the 1999 Kocaeli and 2002 Denali earthquakes to assess whether the sparse near-fault ground motions recorded during these earthquakes are representative of the median level of near-fault ground motions that they caused. If we conclude that they are representative of the median ground motion levels, then the inclusion of these recordings in the data set used to develop the NGA models has not biased them, and our confidence in the NGA models for use in the National Seismic Hazard Maps will be enhanced. However, if we conclude that the recorded ground motions are biased low, then our confidence in the NGA models will be reduced.

The approach to addressing this issue consists of three steps. In the first step, we perform broadband simulations of the recorded near fault ground motions of the two earthquakes, and verify that we are able to simulate the ground motion levels without significant bias. Much of this work has already been done. In the second step, we simulate the near fault ground motions on a grid of stations extending the length of the rupture zone of each event. In the third step, we use these simulations to estimate the median ground motion level along the length of the rupture zone, compare this with the recorded ground motion levels, and determine whether the recorded ground motions provide a biased or unbiased estimate of the expected ground motion levels.

This analysis results in the conclusion that the ground motion recordings of recent large earthquakes, and the NGA ground motion models derived from them, are not biased low in their prediction of ground motion levels from large crustal earthquakes. This provides confidence in the use of the NGA models by the USGS in generating the next revision of the National Seismic Hazard Maps, as well as by other users.

INTRODUCTION

At short and intermediate periods (0.3-3.0s), the recorded ground motions from recent large crustal earthquakes, such as the Mw 7.6 1999 Chi-Chi, Taiwan, Mw 7.4 1999 Kocaeli (Izmit), Turkey and Mw 7.9 2002 Denali, Alaska earthquakes are systematically weaker than those predicted by ground motion models that are currently in use, such as those summarized in Abrahamson and Shedlock (1997). These ground motion recordings have been combined with other strong motion data and used to produce a new generation of ground motion models in the Next Generation Attenuation (NGA) Program (Abrahamson, 2006; Atkinson, 2006; Campbell and Bozorgnia, 2006; Chiou and Youngs, 2006; Idriss, 2006). The NGA ground motion models are based on a much larger and better documented data set that contains many more recordings of earthquakes larger than magnitude 7, compared with the previous generation of models, summarized by Abrahamson and Shedlock (1997), which were used in the current maps.

Inclusion of these recordings in the development of the NGA models has lead to reductions by amounts ranging from 15 – 30% in the levels of ground motions predicted for large earthquakes. Moreover, for most of the NGA models, the strong motion data for the recent large earthquakes required oversaturation at short periods and close distances, that is, ground motion level decreasing with increasing magnitude above about magnitude 7. These NGA models were constrained not to oversaturate, but they do saturate at about magnitude 7, i.e. short period near fault ground motions stop increasing with magnitude above M 7.

Such saturation can be explained using strong motion simulations based on self-similar scaling of rupture area with seismic moment (Frankel, 2006). However, for most of the NGA models, the strong motion data for the recent large earthquakes required oversaturation, and there is concern that this tendency for oversaturation is a symptom of bias in the sparse strong motion recordings of these recent large earthquakes. Frankel (2006) analyzed regional and teleseismic seismograms of these earthquakes and their aftershock sequences and found no evidence for increase in the falloff of short period spectra at large magnitude that would indicate some change in behavior (such as fault lubrication) at large magnitudes that might cause oversaturation.

The objective of this project is to use broadband ground motion simulations of the 1999 Kocaeli and 2002 Denali earthquakes to assess whether the sparse near-fault ground motions recorded during these earthquakes are representative of the average level of near-fault ground motions that they caused. The proposed approach to addressing this issue consists of three steps. In the first step, we perform broadband simulations of the recorded near fault ground motions of the two earthquakes, and verify that we are able to simulate the ground motion levels without significant bias. In the second step, we simulate the near fault ground motions on a grid of stations extending the length of the rupture zone of each event. In the third step, we use these simulations to estimate the median ground motion level along the length of the rupture zone, compare this with the recorded ground motion level, and determine whether the recorded ground motions provide a biased or unbiased estimate of the expected ground motion levels.

The focus of this report is on the 1999 Kocaeli and 2002 Denali earthquakes. Another earthquake of concern to the USGS hazard mapping team is the 1999 Chi-chi, Taiwan earthquake, whose ground motions were lower than current models. This earthquake was well recorded on strong motion instruments, and the concern relates to the uneven distribution of recording stations, which may oversample the weaker short period wave field to the north and undersample the stronger short period wave field to the south, and oversample the weaker ground motions on the foot wall to the west and undersample the stronger ground motions on the hanging wall to the east. This event is not included in our study because we think these issues can be resolved by data analysis without the use of simulations.

BROADBAND STRONG MOTION SIMULATION PROCEDURE

We have developed and tested simple kinematic representations of the differences in source parameters, such as slip velocity and rupture velocity, between the shallow and deep parts of the rupture that are able to reproduce the observed differences in ground motions between shallow and buried faulting earthquakes, using the broadband simulation procedure of Graves and Pitarka (2004). We use a slip velocity function that is constructed using two triangles as shown in Figure 1. This functional form is based on results of dynamic rupture simulations (Guatteri et al., 2003). We constrain the parameters of this function as follows:

$$T_r = 1.6 \times 10^{-9} \cdot M_0^{-1/3} \quad depth < 5km$$

$$T_r = 3.2 \times 10^{-9} \cdot M_0^{-1/3} \quad depth > 5km$$

$$T_p = 0.2 \cdot T_r$$

$$h = 0.2 \cdot A$$

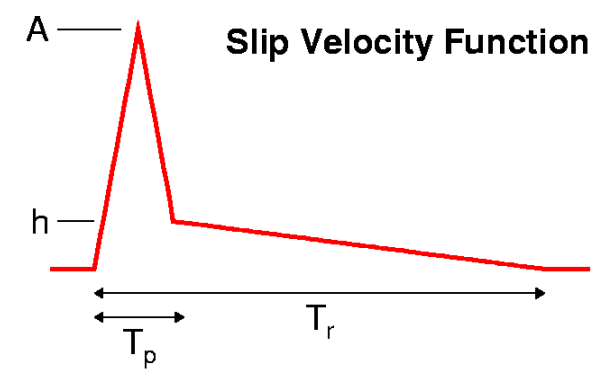

Figure 1. Slip velocity function used in the deterministic simulations.

where M_0 is the seismic moment, T_r is the rise time and A is normalized to give the desired final slip. The expression for T_r comes from the empirical analysis of Somerville et al. (1999). In general, T_r may vary across the fault; however, in practice we only allow a depth dependent scaling such that T_r increases by a factor of 2 if the rupture is between 0 and 5 km depth. This is consistent with observations of low slip velocity on shallow fault ruptures that we describe in the Appendix (Figure A4).

The rupture initiation time (T_i) is determined using the expression

$$T_i = R / V_r - \delta t$$

$$V_r = 0.8 \cdot V_s$$

where R is the rupture path length from the hypocenter to a given point on the fault surface, V_r is the rupture velocity and is set at 80% of the local shear wave velocity (V_s), and δt is a timing perturbation that scales linearly with slip amplitude such that $\delta t = \delta t_0$ where the slip is at its maximum and $\delta t = 0$ where the slip is at the average slip value. For these calculations, we set $\delta t_0 = 0.1\text{sec}$. This scaling results in faster rupture across portions of the fault having large slip as suggested by source inversions of past earthquakes (Hisada, 2001).

Validation of Broadband Ground Motion Simulation Procedure

An example of the testing and application of this simulation procedure is shown in Figure 3, which compares the recorded (black) and simulated (red) velocity waveforms of the 1989 Loma Prieta earthquake at six stations. The amplitude and phasing of the recorded waveforms is generally well matched by the simulations. The goodness of fit in spectral acceleration between the recorded and simulated time histories for 21 recordings of the 1999 Izmit (Kocaeli) earthquake is quantified in Figure 3. The solid red line shows the bias, i.e. the median value of the residuals (data minus simulation), which is not significantly different from zero at the 90% confidence level, shown by the dashed black lines. This means that averaged over all 21 stations, the simulation procedure neither over-predicts nor under-predicts the recorded ground motions. The standard error of the scatter of the individual residuals about this median value is shown by the dashed green lines. The standard error of about a factor of 1.5 (0.4 natural log units) means that at a specific station, the difference between the recorded and simulation ground motion at a particular response spectral period has a standard error of a factor of 1.5.

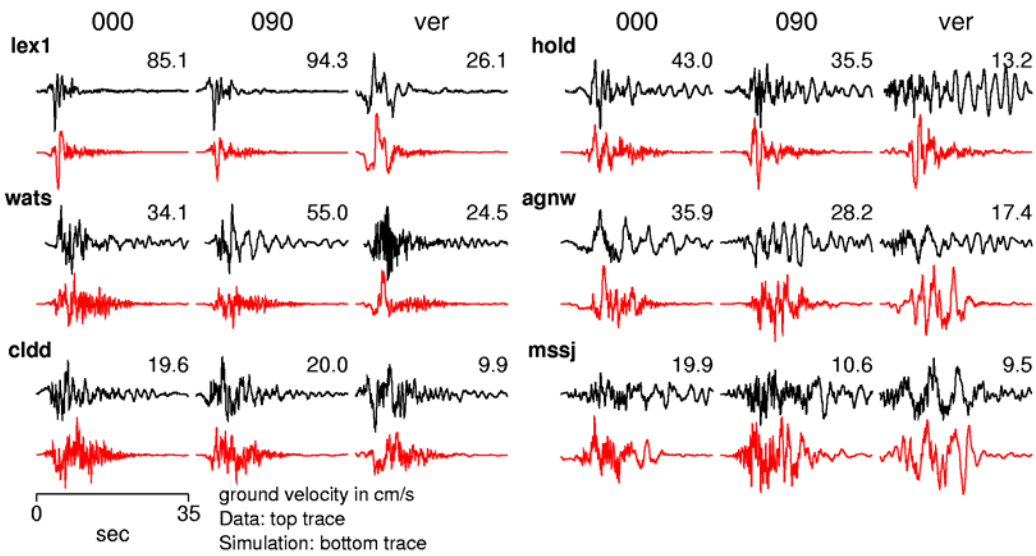

Figure 2. Comparison of observed (black) and simulated (red) broadband 3-component ground velocity records at six sites for the Loma Prieta earthquake. Source: Graves and Pitarka (2004).

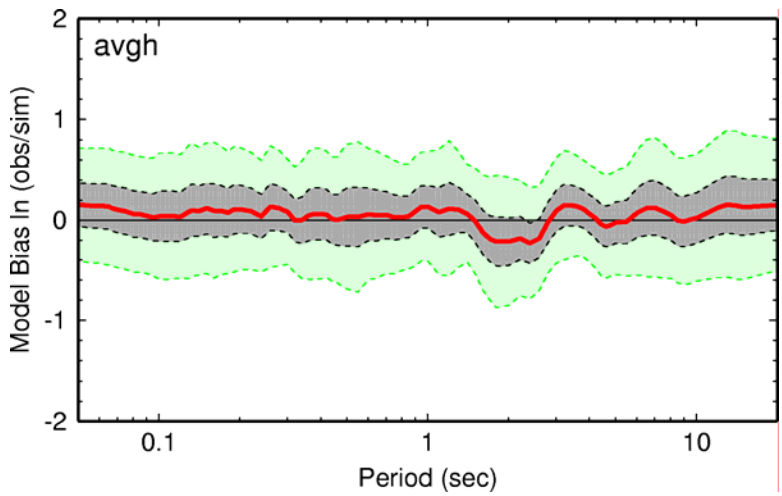

Figure 3. Performance of the simulation procedure in matching the 5% damped response spectra of the 1999 Kocaeli earthquake recorded at 21 stations. The red line shows the natural logarithm of the model bias (data – simulation) and the black dotted lines show its 90% confidence interval. The green lines show the natural logarithm of the standard error.

The performance of the procedure in modeling five crustal earthquakes, including the 1979 Imperial Valley, 1989 Loma Prieta, 1992 Landers, 1994 Northridge, and 1999 Kocaeli, Turkey, earthquakes is summarized in Figures 4 and 5. Two events have buried faulting (Loma Prieta and Northridge), and the other three have surface rupture. Figure 4 shows the bias as a function of period for each of the five earthquakes. The lack of systematic bias indicates that the scaling of slip velocity with depth that is used in the simulation procedure accurately reproduces the trends in the data. Without this scaling, the simulation would produce systematic biases, such as those shown in the Appendix in Figure A2 with respect to the Abrahamson and Silva (1997) model which does not distinguish between surface and buried rupture events. The top panels of Figure 5 show the residuals for each site and each event (color coded) as a function of closest distance to the fault for response spectral periods of 0.3, 1 and 3 seconds. The bottom panels show event-averaged residuals as a function of magnitude. There is no systematic bias in

the near-fault simulation of these data, which span magnitudes from 6.6 to 7.4 and include both buried and surface rupture events.

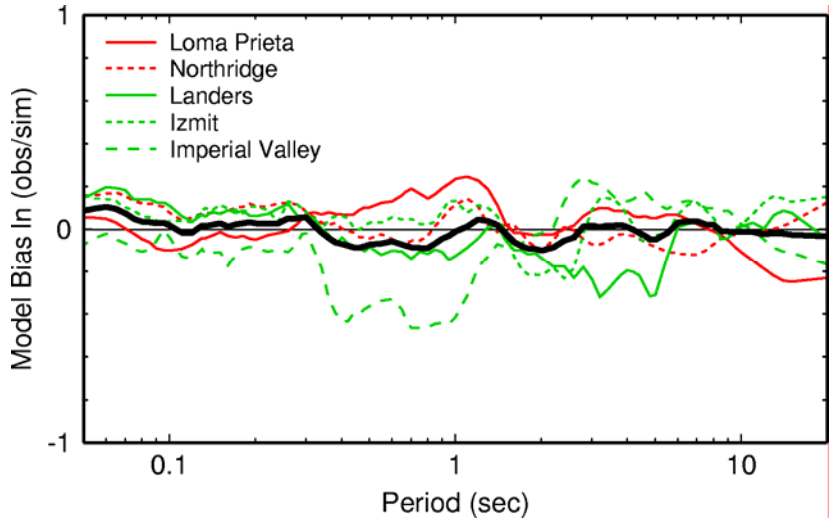

Figure 4. Residuals between recorded and simulated spectral acceleration for five earthquakes, and average over the five (black line). The simulation procedure predicts the recorded ground motions without significant bias for both surface and buried faulting events. If the simulation procedure did not account for differences between surface and buried faulting events, the residuals would resemble those in Fig. 3. Izmit denotes the Kocaeli earthquake.

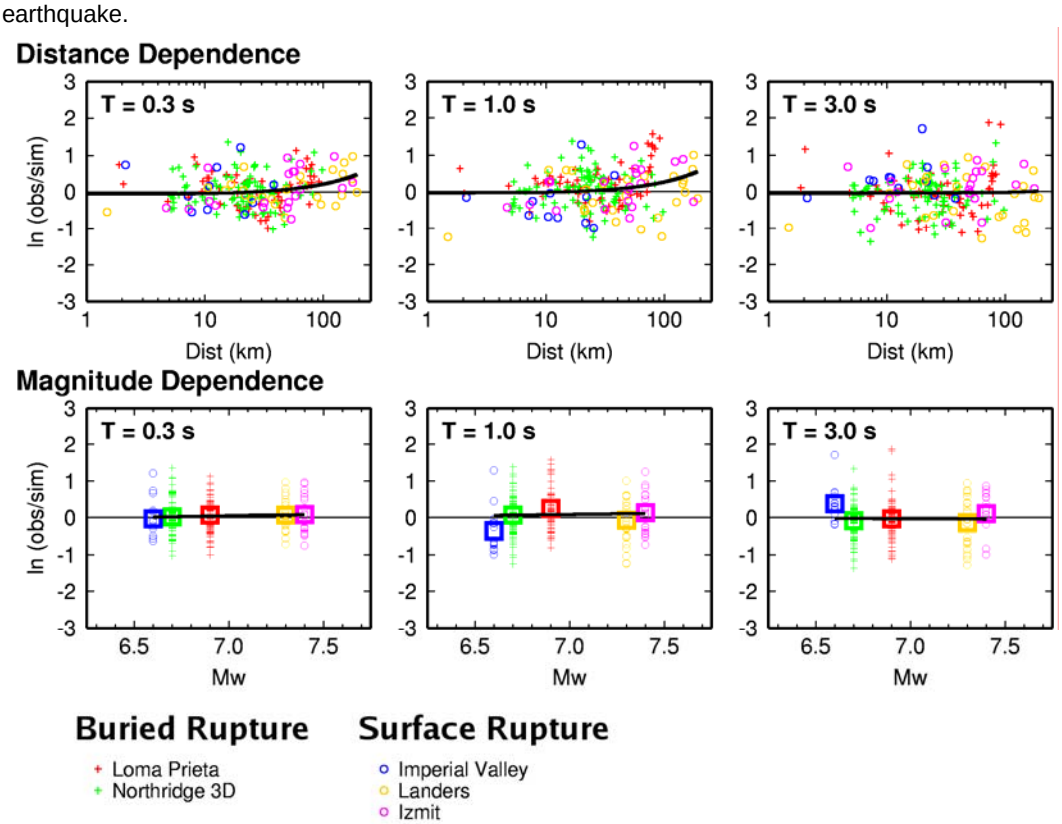

Figure 5. Residuals between recorded and simulated spectral acceleration at periods of 0.3, 1, and 3 seconds for 5 earthquakes. Each point represents one recording station, with the different earthquakes coded by color. Surface rupture events are indicated by circles and buried rupture events by crosses. Top panels show residuals versus closest distance to the rupture, and bottom panels show residuals versus magnitude. The simulation procedure predicts the recorded near-fault ground motions without significant bias for both surface and buried faulting events. Izmit denotes the Kocaeli earthquake.

METHOD

The objective of this project is to use broadband ground motion simulations of the 1999 Kocaeli and 2002 Denali earthquakes to assess whether the sparse near-fault ground motions recorded during these earthquakes are representative of the average level of near-fault ground motions that they caused. The approach to addressing this issue consists of three steps. In the first step, we collected rupture models of the two earthquakes, their strong motion recordings, and information about the near surface shear wave velocities at the recording stations. The near surface shear wave velocity at PS10 near the Denali fault and at the near-fault strong motion stations along the Kocaeli rupture are described in special earthquake reconnaissance issues for each event (Youd et al., 2000; Haeussler and Naeim, 2004), and Vs30 values are provided in the NGA Flatfile. We obtained crustal seismic velocity models for both regions used in the rupture velocity inversions, and calculated Green's functions for these models.

In the second step, we performed broadband simulations of the recorded near fault ground motions of the two earthquakes, and verified that we are able to simulate the ground motion levels without significant bias. The results of this work are described above in Figures 2 through 5.

In the third step, we simulated the near fault ground motions on a grid of stations extending the length of the rupture zone of each event. These simulations were done for a uniform near surface reference velocity. The recorded ground motions were adjusted to the reference velocity using the method described by Graves and Pitarka (2004).

In the fourth step, we used these simulations to estimate the median ground motion level along the length of the rupture zone, compared this with the recorded ground motion level, and determined whether the recorded ground motions provide a biased or unbiased estimate of the expected ground motion levels. Due to the sparsity of near fault recordings of the Denali earthquake, there is limited opportunity to check the absolute levels of our simulated ground motions against recorded levels, but by comparing the levels of simulated ground motions at PS10 with those at other locations along the fault, we can establish whether the PS10 recording is representative of the ground motion level averaged along the fault at that distance from the fault.

2002 DENALI EARTHQUAKE

The rupture models of the Denali earthquake, listed in Table 1, were in most cases derived from a combination of different kinds of data. The surface traces of the five fault models are compared in Figure 6, and the individual rupture models are shown in Figure 7. Of the five models, all used at least two data categories. Use of these five rupture models is expected to avoid the bias that might be present if we were to only use one rupture model, or to use rupture models that were derived exclusively from strong motion data.

Table 1. Rupture Models of the Denali Earthquake

Earthquake	Authors	Data Categories used in Rupture Model Inversion
Denali	Asano et al. (2005)	GPS, strong motion
	Dreger et al. (2004)	Regional seismograms, GPS, surface offsets
	Ji (Tsuboi et al., 2003)	Teleseismic body waves, surface offsets
	Oglesby et al. (2004)	Regional seismograms, GPS, surface offsets
	Thio (2003)	Teleseismic body and surface waves

There was only one near-fault strong motion recording of the Denali earthquake (Pump Station 10 at 2.74 km from the fault, shown in Figure 6 and listed in Table 2), and so the rupture models of this earthquake are not strongly constrained by strong motion data. There is concern that the PS10 station was located near a segment of the Denali fault that experienced less displacement than the average displacement along the fault, and where supershear rupture velocity may have also reduced the ground motion level, with the result that the PS10 recording yields an estimate of the ground motions at a distance of 2.74 km from the Denali fault rupture that is biased low. Due to the sparsity of strong motion data for this earthquake, there is limited opportunity to check the absolute levels of our simulated ground motions against recorded levels, but by comparing the levels of simulated ground motions at PS10 with those at other locations along the fault, we expect that we can establish whether the PS10 recording is representative of the ground motions level averaged along the fault at that distance from the fault.

Table 2. Closest distance and Vs30 for recordings of the 2002 Denali Earthquake

Station	Vs30 (m/sec)	Closest Distance (average of 5 slip models)	Closest distance (NGA)
PS10	329 m/sec	3.28 km	2.74 km

The individual ground motions from each grid point (dots) and the fit to these points (black line) are compared with the recorded and simulated values at PS10, adjusted to Vs30 of 1,000m/sec in Figures 8 through 13. Figure 8 shows the results for the average of the five rupture models, and Figures 9 through 13 show the results for the individual rupture models. The average in Figure 8 uses the average distance of PS10 from the five fault models.

The simulated values at PS10 are in close agreement with the average simulated values for that distance at all periods (represented by the black line), indicating that the location of PS10 is not expected to bias the PS10 recording either high or low.

The recorded values at PS10 are lower than the average simulated values for that distance at periods of 0.5 seconds and less, and in close agreement at longer periods. This kind of variability is typical of individual recordings, and we do not have enough recordings to be able to test the significance of the difference between the recorded values and the simulations at short periods.

Figures 14 through 19 show the same information as Figures 8 through 13, with the addition of ground motion predictions from three NGA models. The NGA models are close to the simulated values at PS10 and to the average values of the simulations for periods of 0.3 seconds and less, and below them for periods longer than 0.3 seconds.

The NGA models are above the recorded values at PS10 for periods of 0.5 seconds and less, above them for periods between 1 and 3 seconds, and comparable to them for periods between 5 and 10 seconds.

Our conclusions from these comparisons are as follows:

The location of PS10 is not expected to bias the PS10 recording either high or low, based on the simulations.

The recorded values at PS10 are lower than both the NGA models and the simulations for periods less than 1 second, and higher than the NGA models and comparable to the simulations for periods between 1 and 5 seconds.

The simulations are comparable to the NGA models at periods of 0.3 seconds and less, and above the NGA models at periods between 0.5 and 5.0 seconds.

The average of the simulations provides a very good fit to the recorded values at PS10 for periods of 1 second and longer. This is the period range in which the rupture models of the earthquakes used in simulating the ground motions are constrained by data.

1999 KOCAELI EARTHQUAKE

The rupture models of the Kocaeli earthquake used in this study, and the categories of data from which they were derived, are listed in Table 3. The surface traces of the Thio (2005) model are shown in Figure 20. The surface traces of the three fault models are compared in Figure 21, and the individual rupture models are shown in Figure 22. Of the three models, all used strong motion recordings, but two used diverse additional data categories. Use of these three rupture models is expected to avoid the bias that might be present if we were to only use one rupture model, or to use rupture models that were derived exclusively from strong motion data.

Table 3. Rupture Models of the Kocaeli Earthquake

Authors	**Data Categories used in Rupture Model Inversion**
Delouis et al. (2002)	InSAR, GPS, teleseismic, strong motion
Sekiguchi et al. (2002)	Strong motion
Thio et al. (2005)	Teleseismic body and surface waves, GPS, strong motion

There are six near-fault recordings, listed in Table 4, distributed along the 150 km of the fault rupture of the Kocaeli earthquake, which involved multiple fault segments. The focus of our study is on whether the locations of the strong motion stations along the fault may provide a biased estimate of the average ground motion levels. For example, two stations (izt and ypt) are located close to the epicenter, and so we expect that they were subject to low or moderate rupture directivity effects, and other stations are located near the ends of the rupture near regions of low slip. The strong spatial variation in slip and other rupture properties and the segmented character of the rupture may have introduced spatial variations in ground motions that were not adequately sampled by the strong motion stations.

Table 4. Closest distance and Vs30 for recordings of the 1999 Izmit Earthquake

Station	Vs30 (m/sec)	Closest Distance (average of 3 slip models)	Closest distance (NGA)
arc	523	13	13.49
dzc	276	11.5	15.37
gbz	792	12.0	10.92
izt	811	7.4	7.21
skr	471	3.4	3.12
ypt	297	4.9	4.83

The individual ground motions from each grid point (dots) and the fit to these points (black line) are compared with the recorded and simulated values at the six recording sites, adjusted to Vs30 of 500m/sec in Figures 23 through 26. Figure 23 shows the results for the average of the three rupture models, and Figures 24 through 26 show the results for the individual rupture models. The average in Figure 23 uses the average distance of the recording stations from the three fault models.

The simulated values at the six recording sites are at or above the level of the average simulated values for that distance at all periods (represented by the black line), indicating that the locations of the six recording stations are not expected to bias them either high or low.

The recorded values at the six recording stations are lower than the average simulated values for that distance at periods of 3 seconds and less, and in close agreement at periods of 5 and 10 seconds. The simulations appear to systematically overestimate the recorded ground motions at periods less than 3 seconds.

Figures 27 through 30 show the same information as Figures 23 through 26, with the addition of ground motion predictions from three NGA models. The NGA models are close to the simulated values at the six recording stations and to the average values of the simulations for periods of 0.5 seconds and less, and below them for periods longer than 0.5 seconds.

The NGA models are above the recorded values at the six recording stations for periods of 0.5 seconds and less, and comparable to them for periods between 1 and 10 seconds.

Our conclusions from these comparisons are as follows:

The locations of six recording stations is not expected to bias them either high or low, based on the simulations.

The recorded values at the six recording stations are slightly lower than both the NGA models and the simulations for periods less than 0.5 second, comparable to the NGA models for periods of 1 second and longer, and lower than the simulations for periods between 1 and 3 seconds.

The simulations are comparable to the NGA models at periods of 0.5 second and less, and above the NGA models at periods between 1 and 5.0 seconds.

The average of the simulations provides a fairly good fit to the recorded values at the six recording stations for periods of 3 seconds and longer. This is part of the period range in which the rupture models of the earthquakes used in simulating the ground motions are constrained by data.

CONCLUSIONS

The ground motion recordings of recent large earthquakes, and the NGA ground motion models derived from them, are not biased low in their prediction of ground motion levels from large crustal earthquakes. This provides confidence in the use of the NGA models by the USGS in generating the next revision of the National Seismic Hazard Maps, as well as by other users.

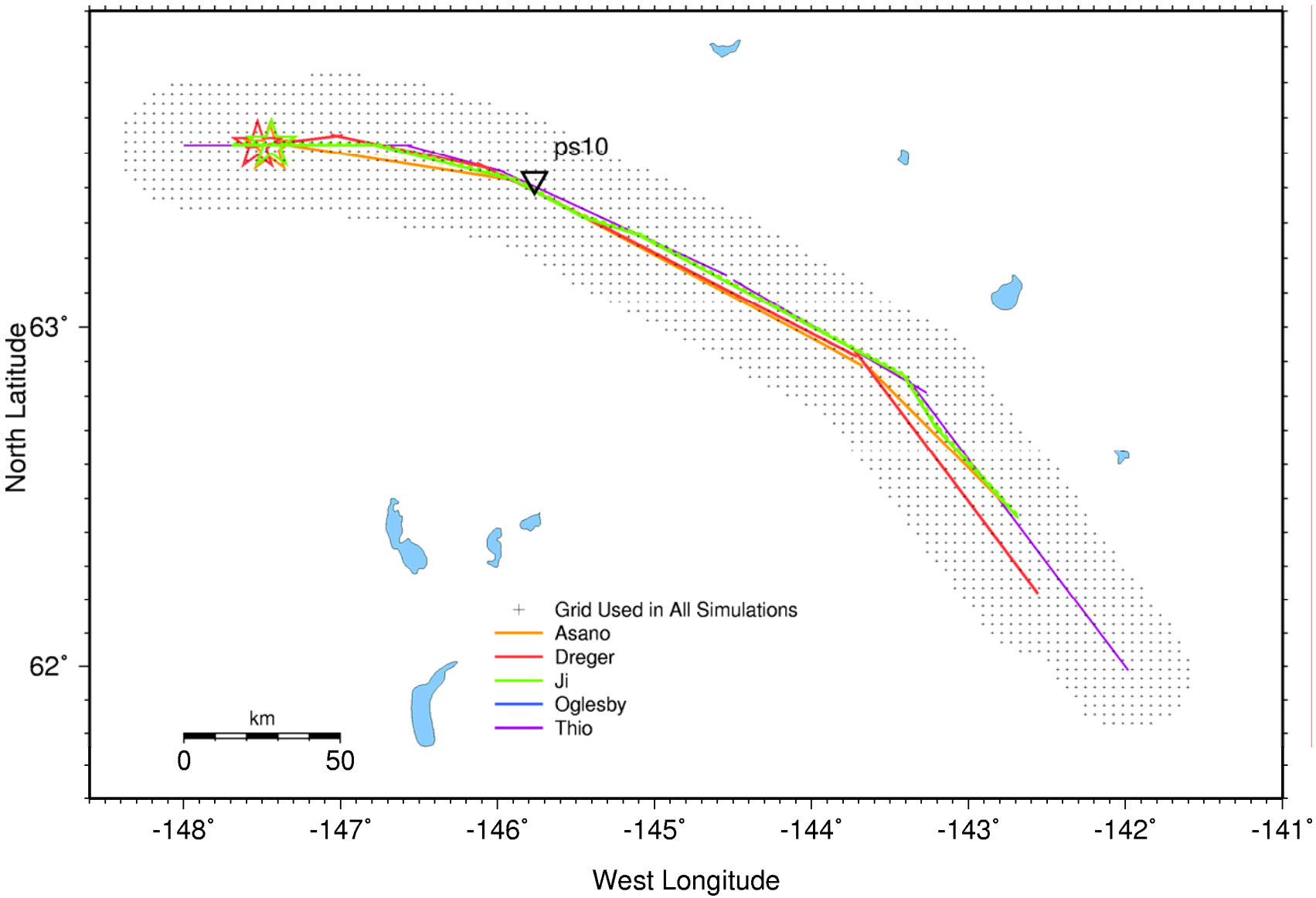

Figure 6. Fault models, recording station locations, and ground motion simulation grid locations for the 2002 Denali earthquake.

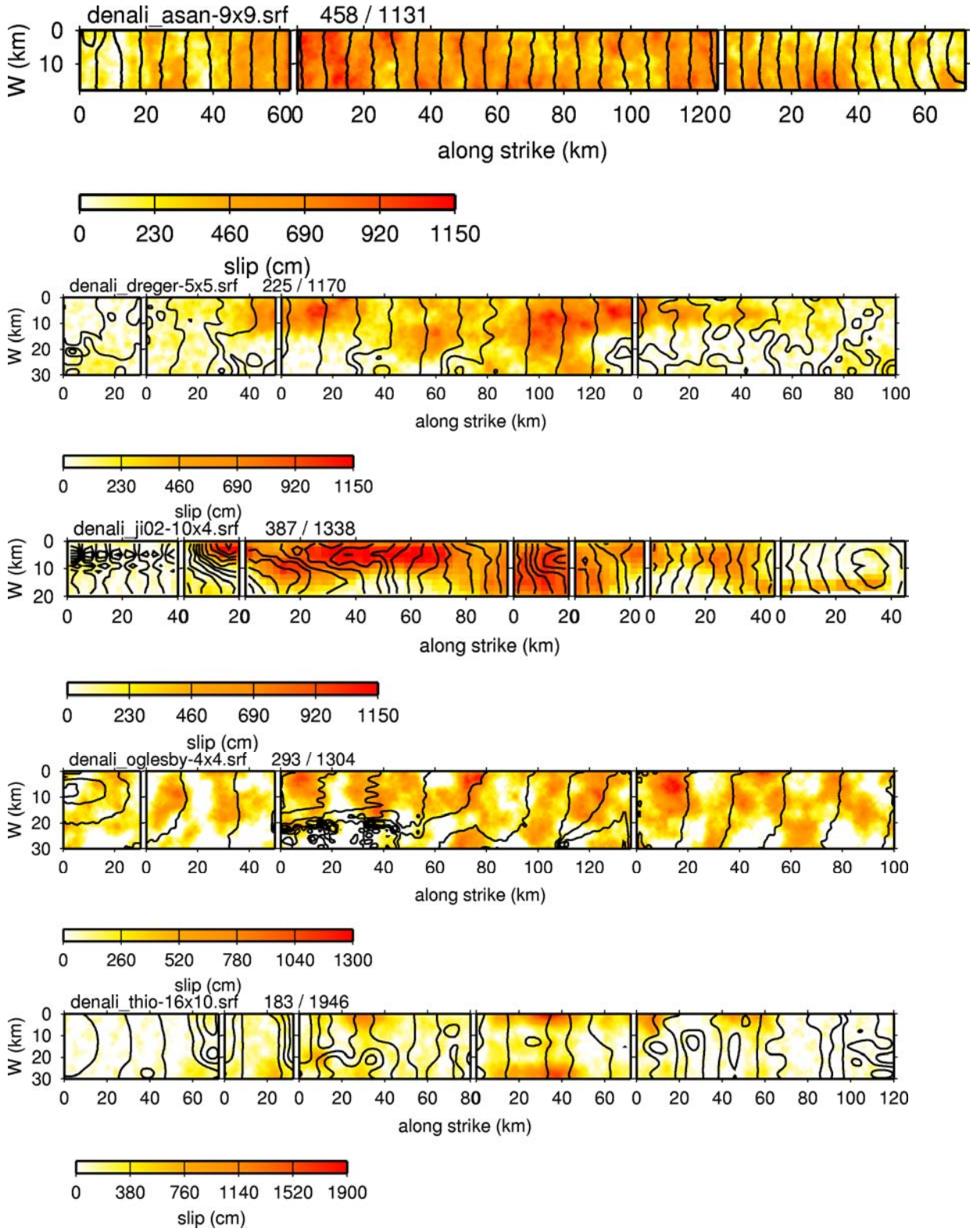

Figure 7. Rupture models (slip and contoured rupture time) of the 2002 Denali earthquake from (top to bottom) Asano, Dreger, Ji, Oglesby, and Thio.

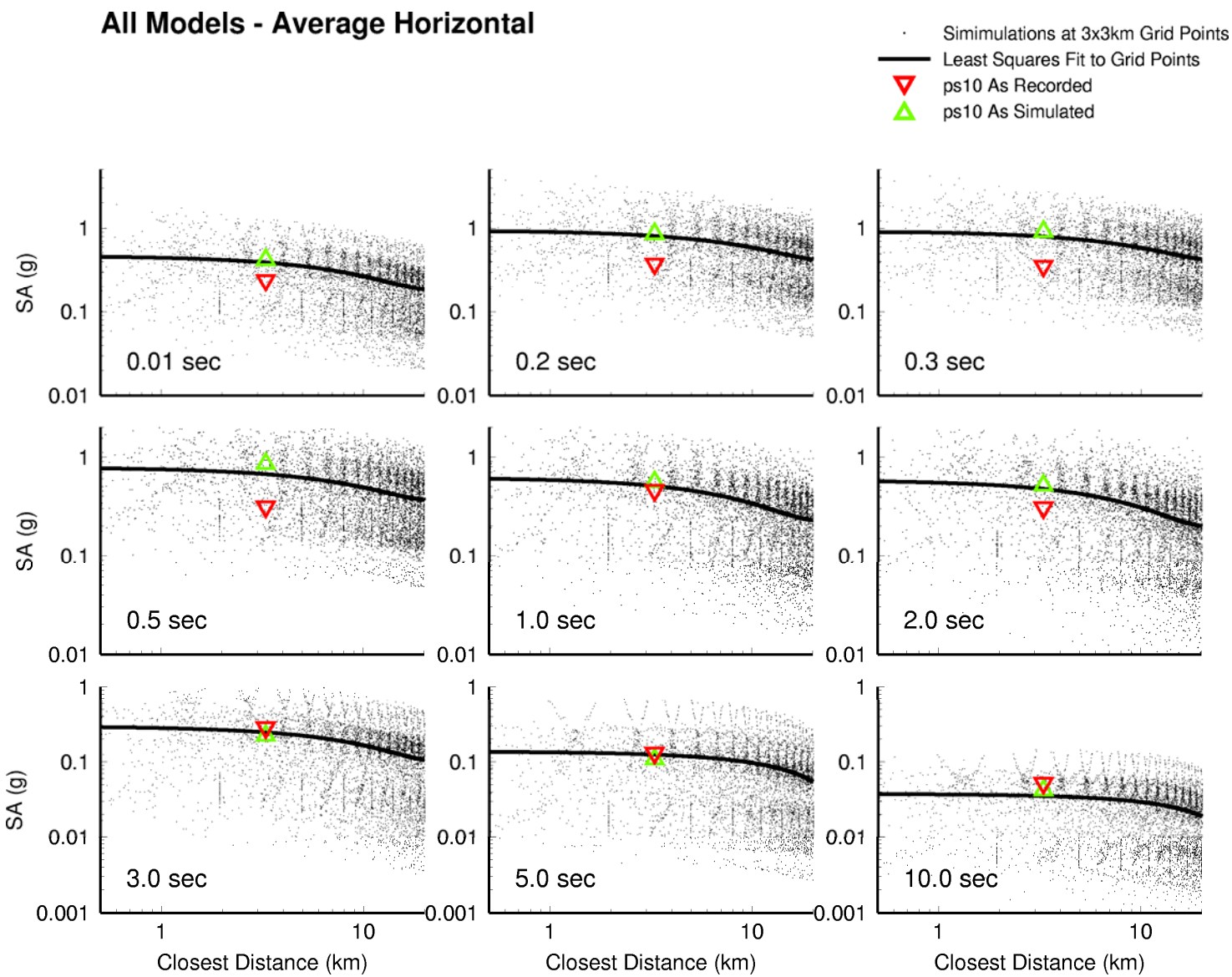

Figure 8. Averaged recorded and simulated ground motions for the five rupture models of the 2002 Denali earthquake.

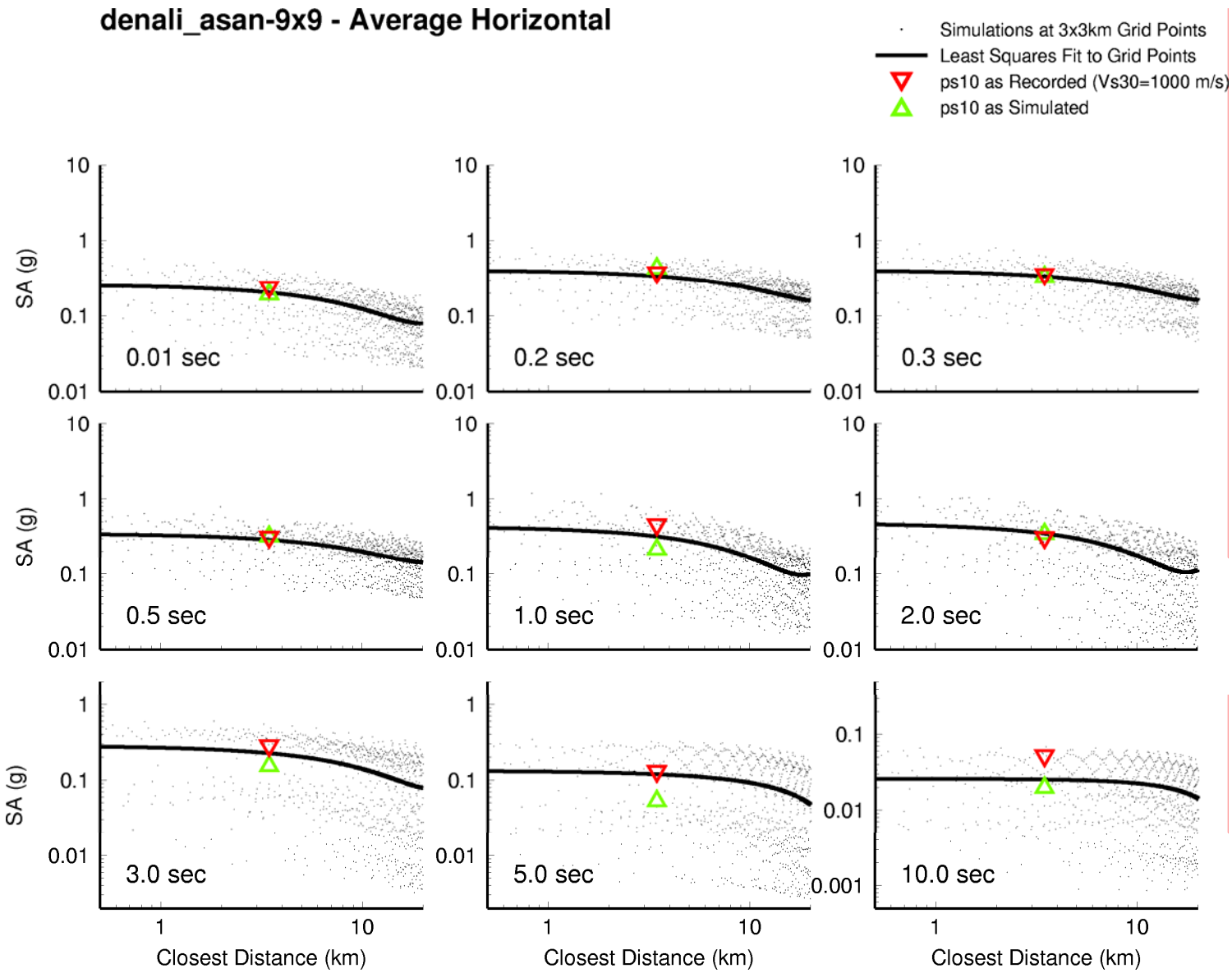

Figure 9. Recorded and simulated ground motions for the Asano et al. (2005) rupture model of the 2002 Denali earthquake.

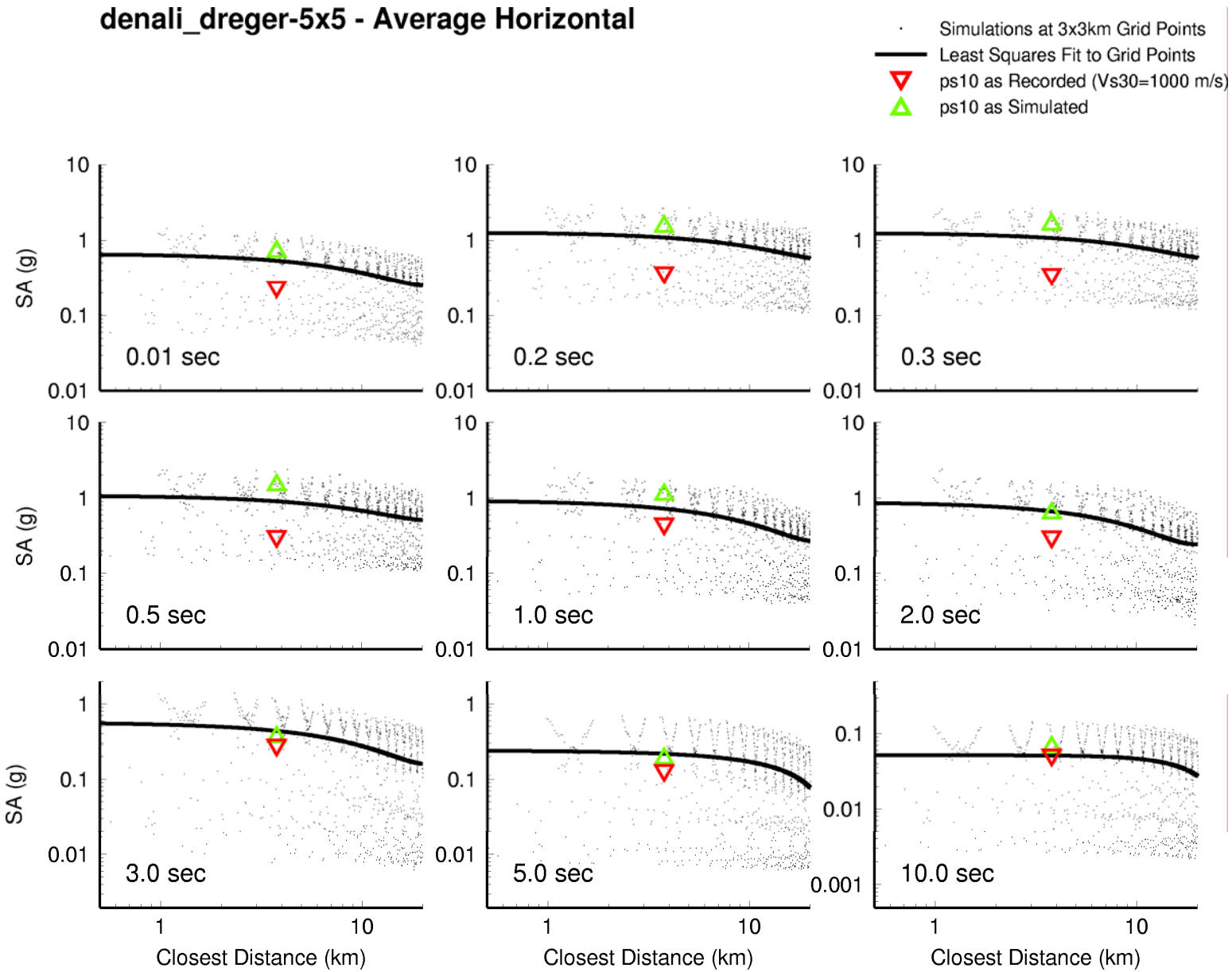

Figure 10. Recorded and simulated ground motions for the Dreger et al. (2004) rupture model of the 2002 Denali earthquake.

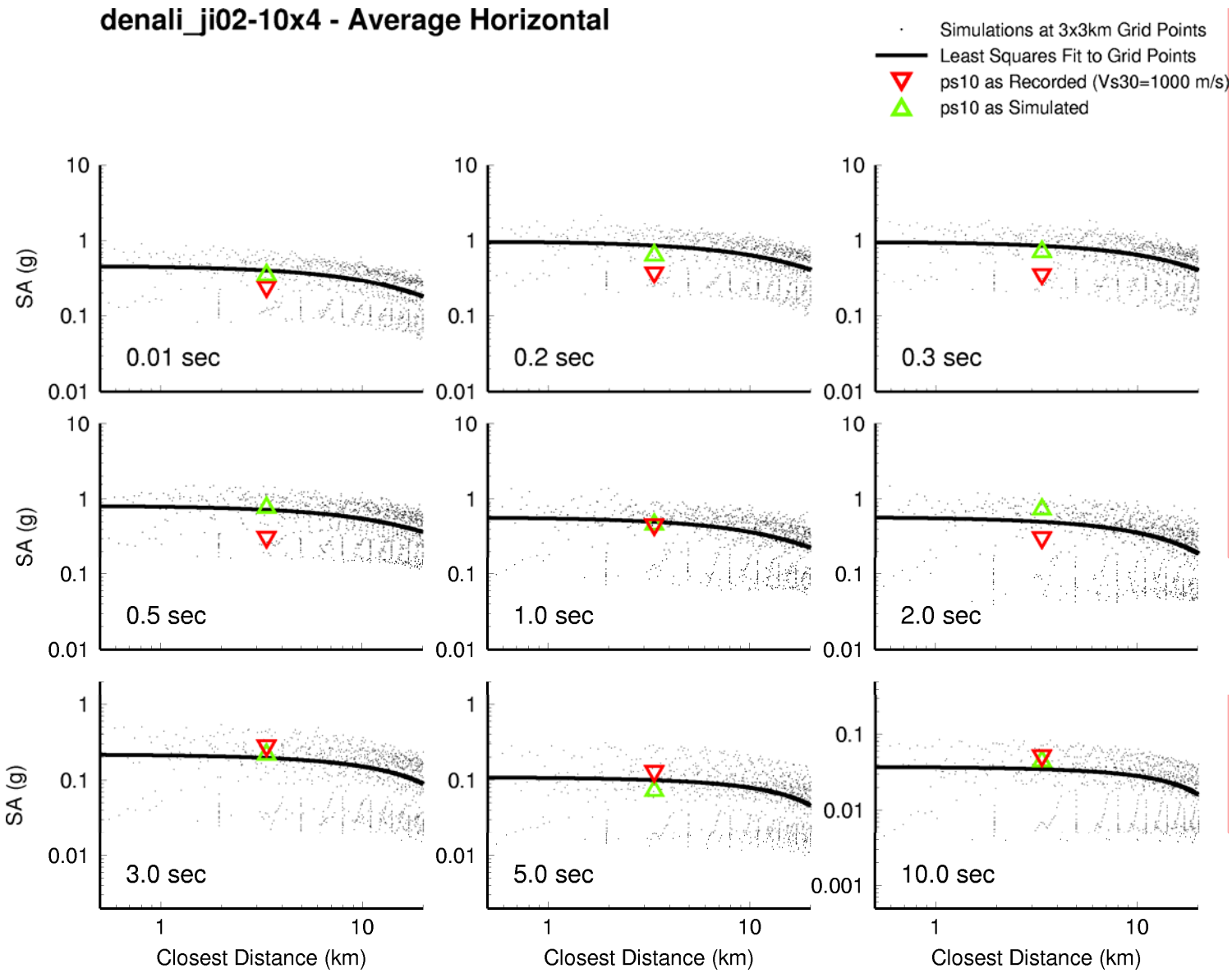

Figure 11. Recorded and simulated ground motions for the Ji et al. (2005) rupture model of the 2002 Denali earthquake.

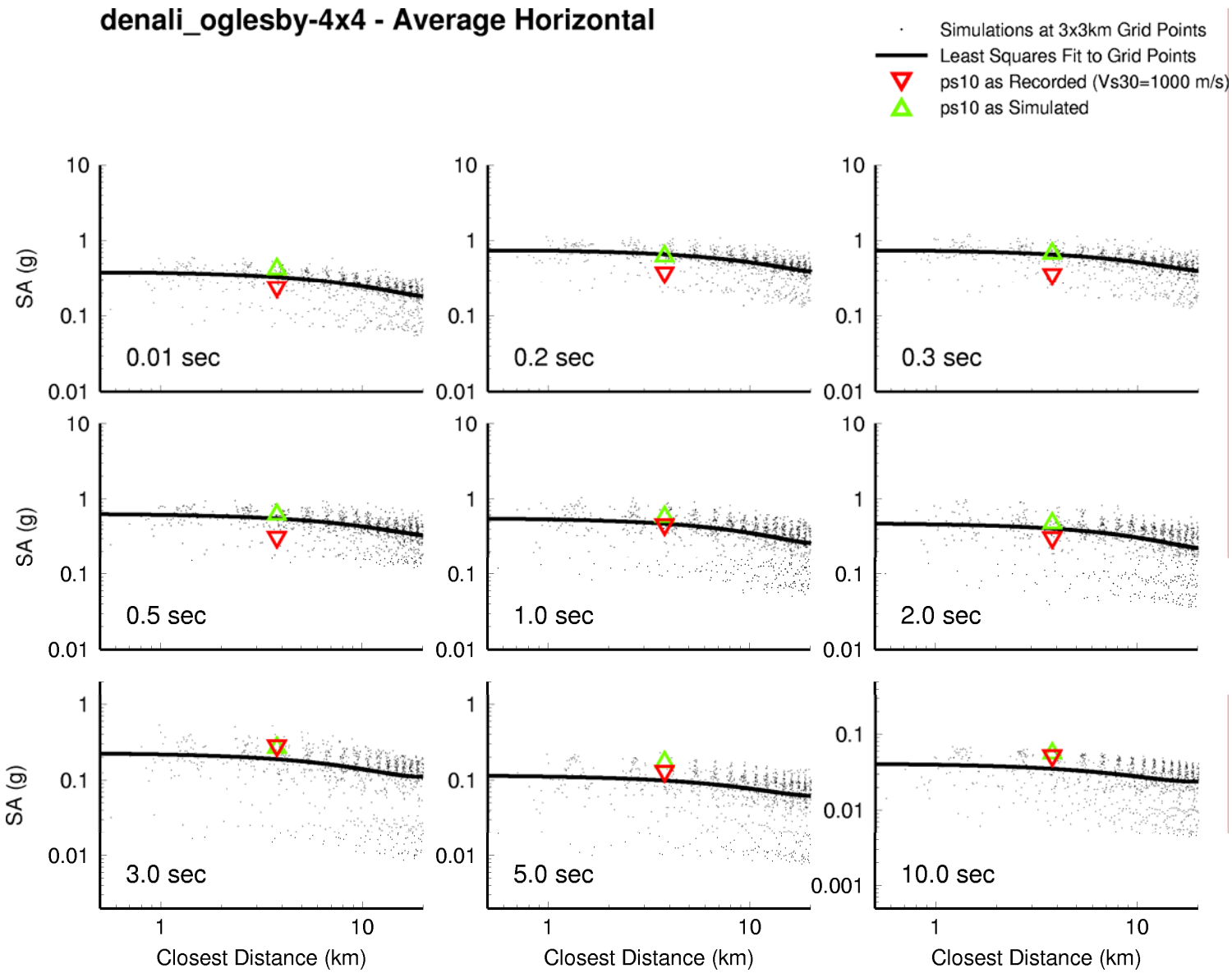

Figure 12. Recorded and simulated ground motions for the Oglesby et al. (2004) rupture model of the 2002 Denali earthquake.

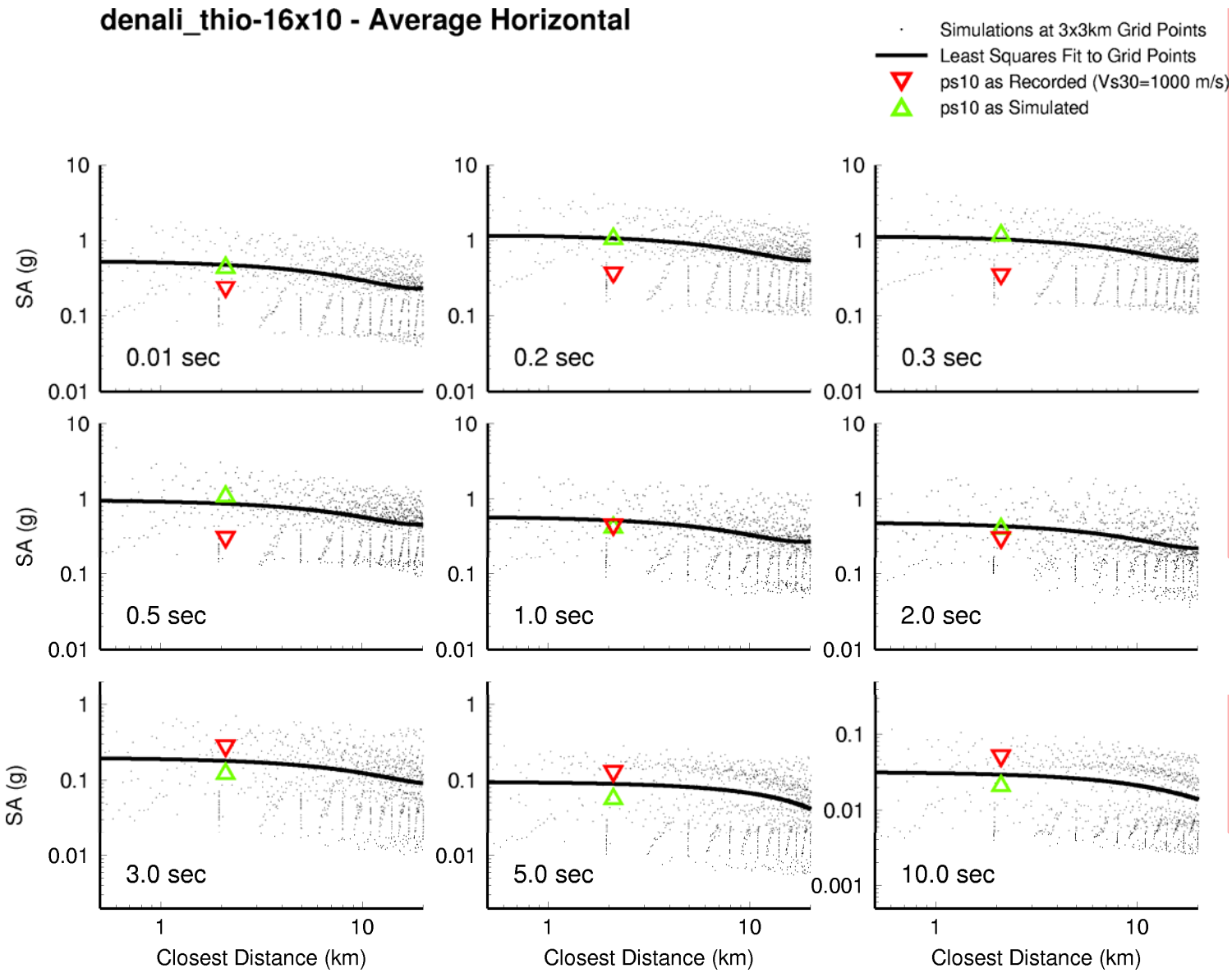

Figure 13. Recorded and simulated ground motions for the Thio (2005) rupture model of the 2002 Denali earthquake.

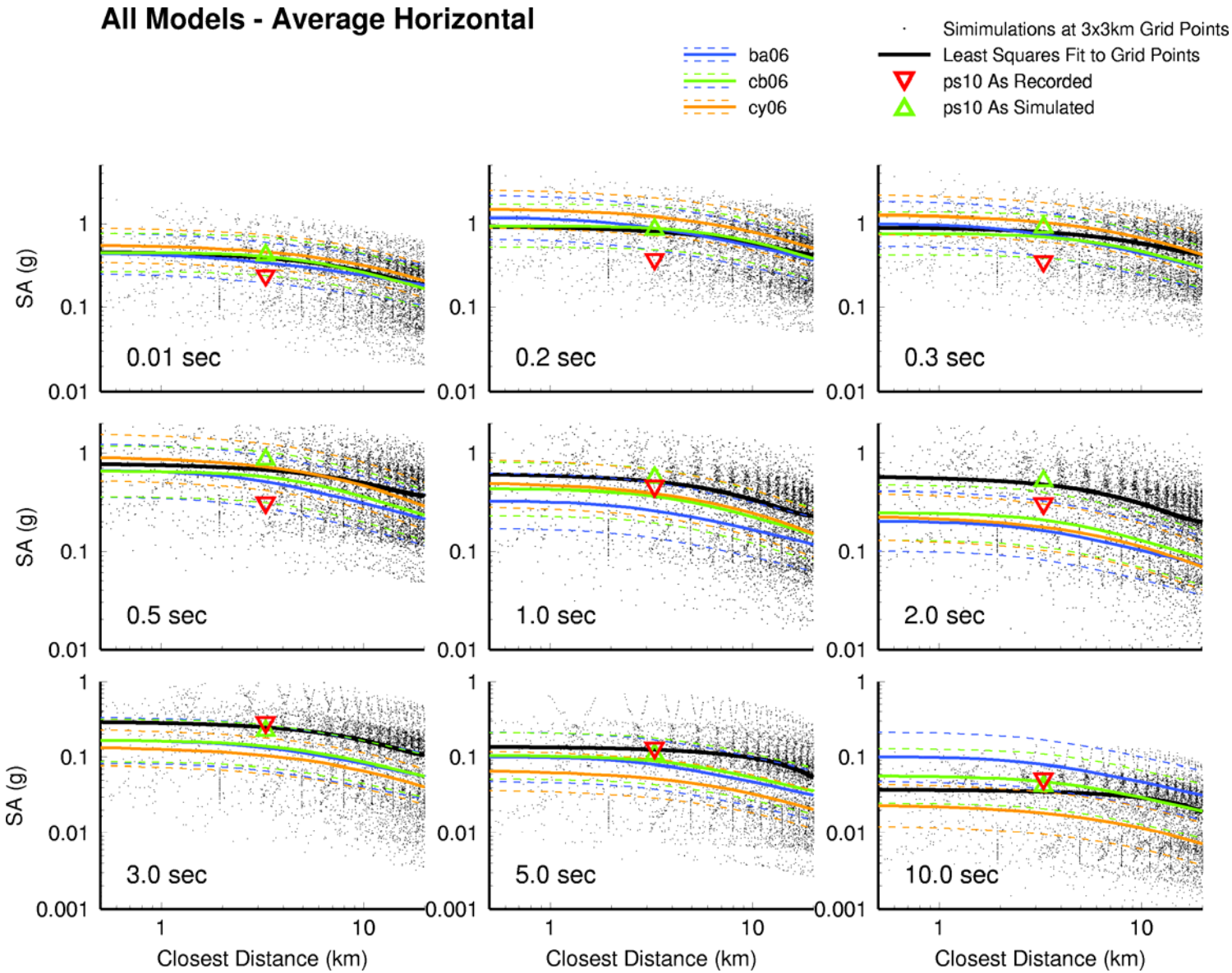

Figure 14. Averaged recorded, simulated and NGA ground motions for the five rupture models of the 2002 Denali earthquake.

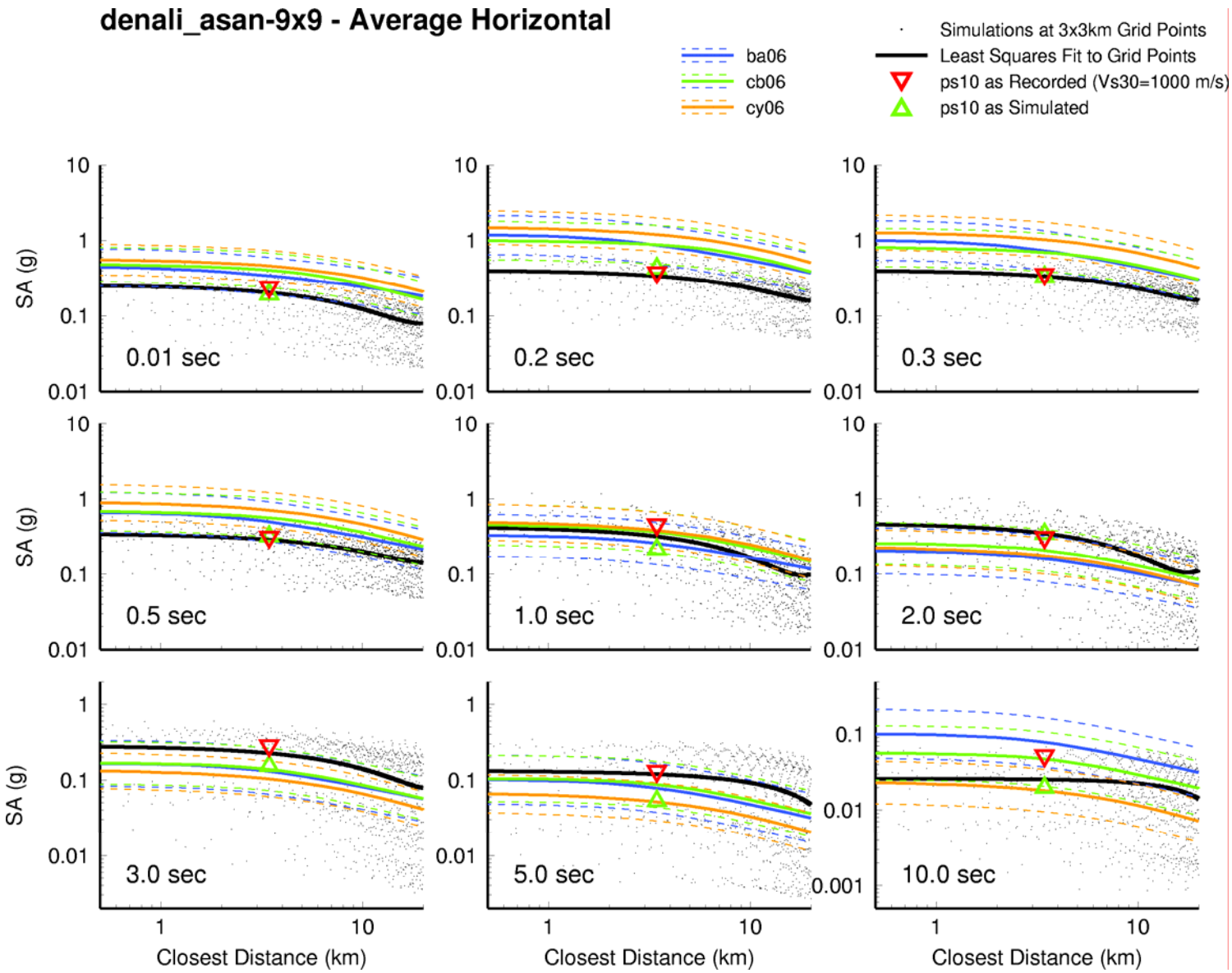

Figure 15. Recorded, simulated and NGA ground motions for the Asano et al. (2005) rupture model of the 2002 Denali earthquake.

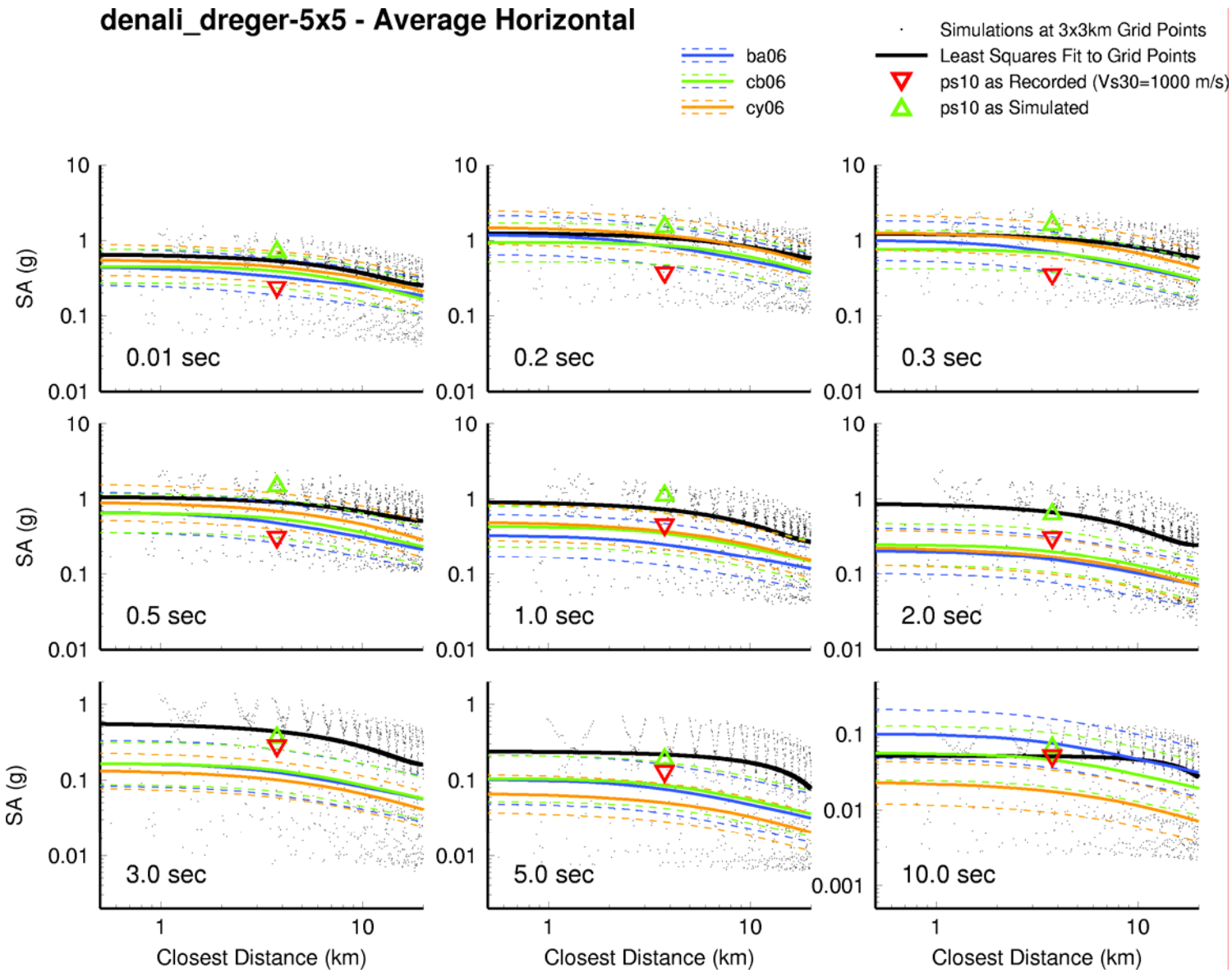

Figure 16. Recorded, simulated and NGA ground motions for the Dreger et al. (2005) rupture model of the 2002 Denali earthquake.

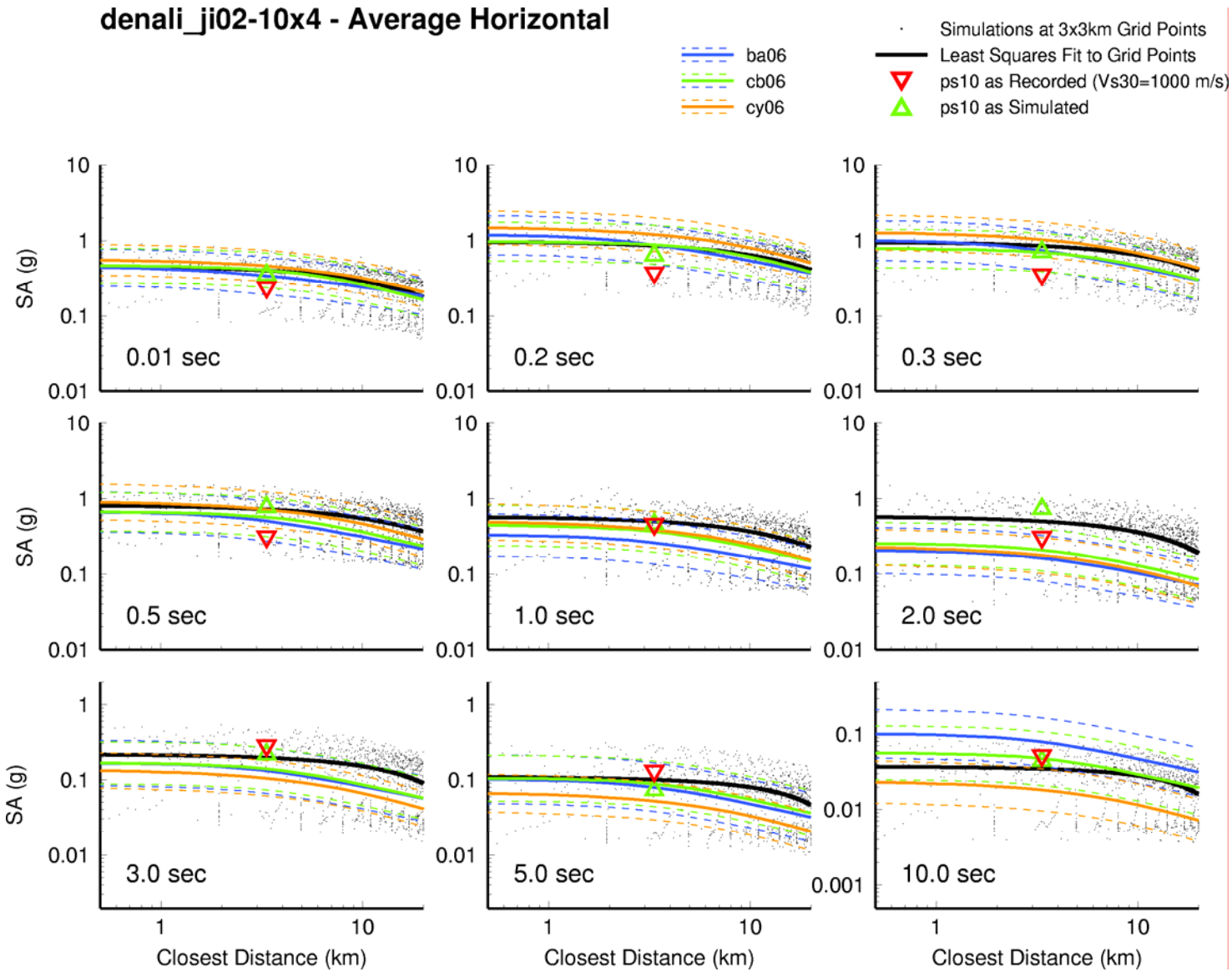

Figure 17. Recorded, simulated and NGA ground motions for the Ji et al. (2005) rupture model of the 2002 Denali earthquake.

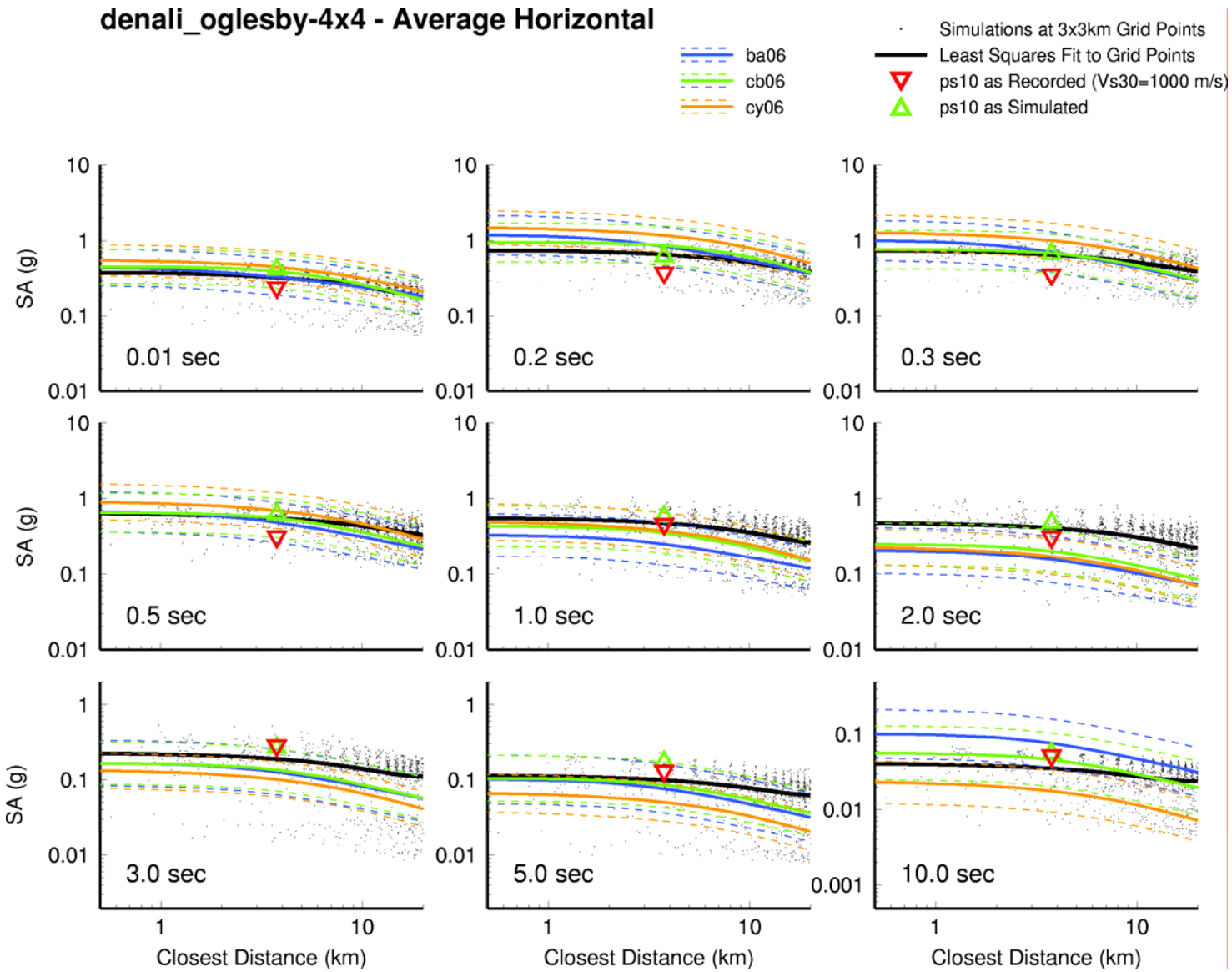

Figure 18. Recorded, simulated and NGA ground motions for the Oglesby et al. (2004) rupture model of the 2002 Denali earthquake.

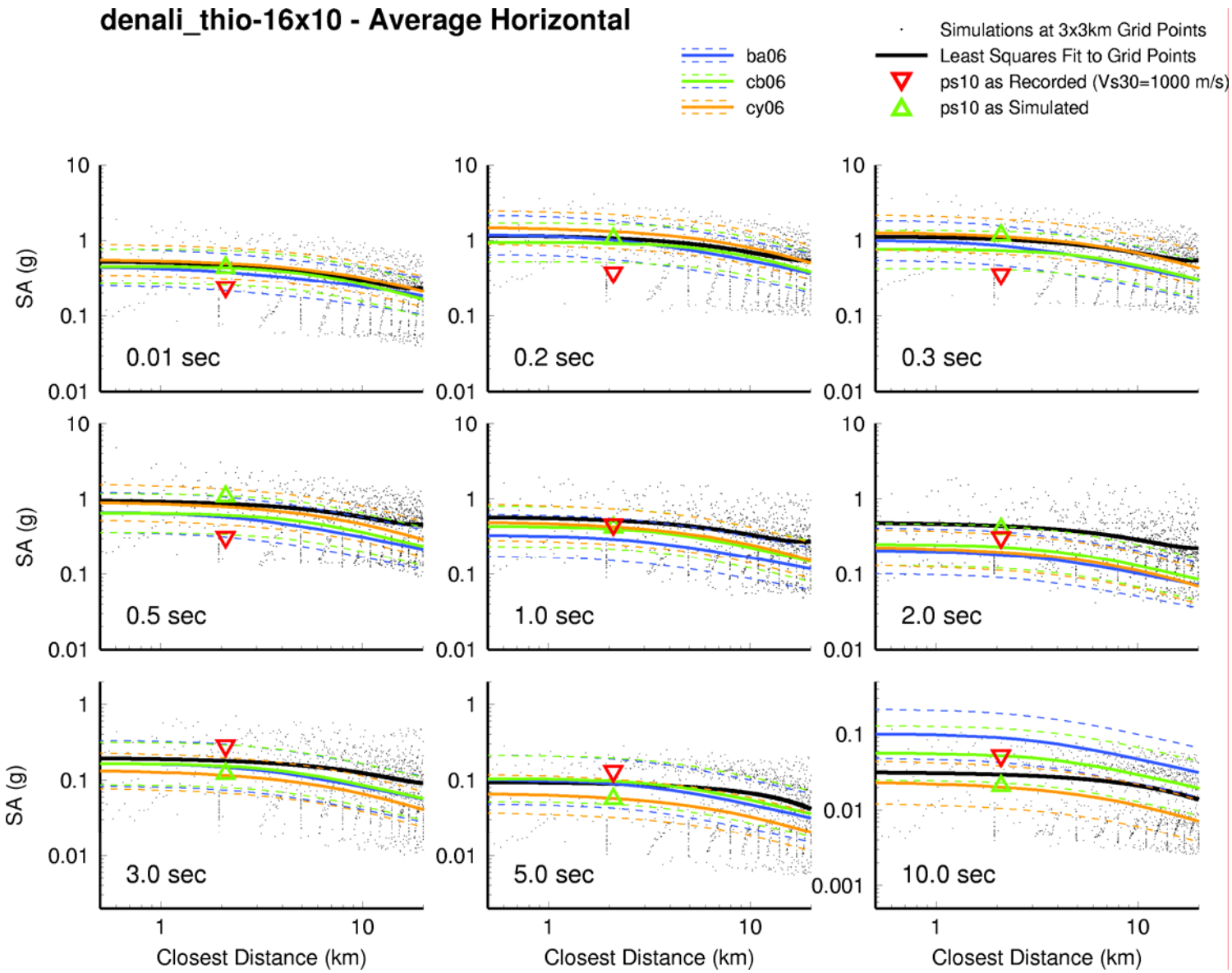

Figure 19. Recorded, simulated and NGA ground motions for the Thio (2005) rupture model of the 2002 Denali earthquake.

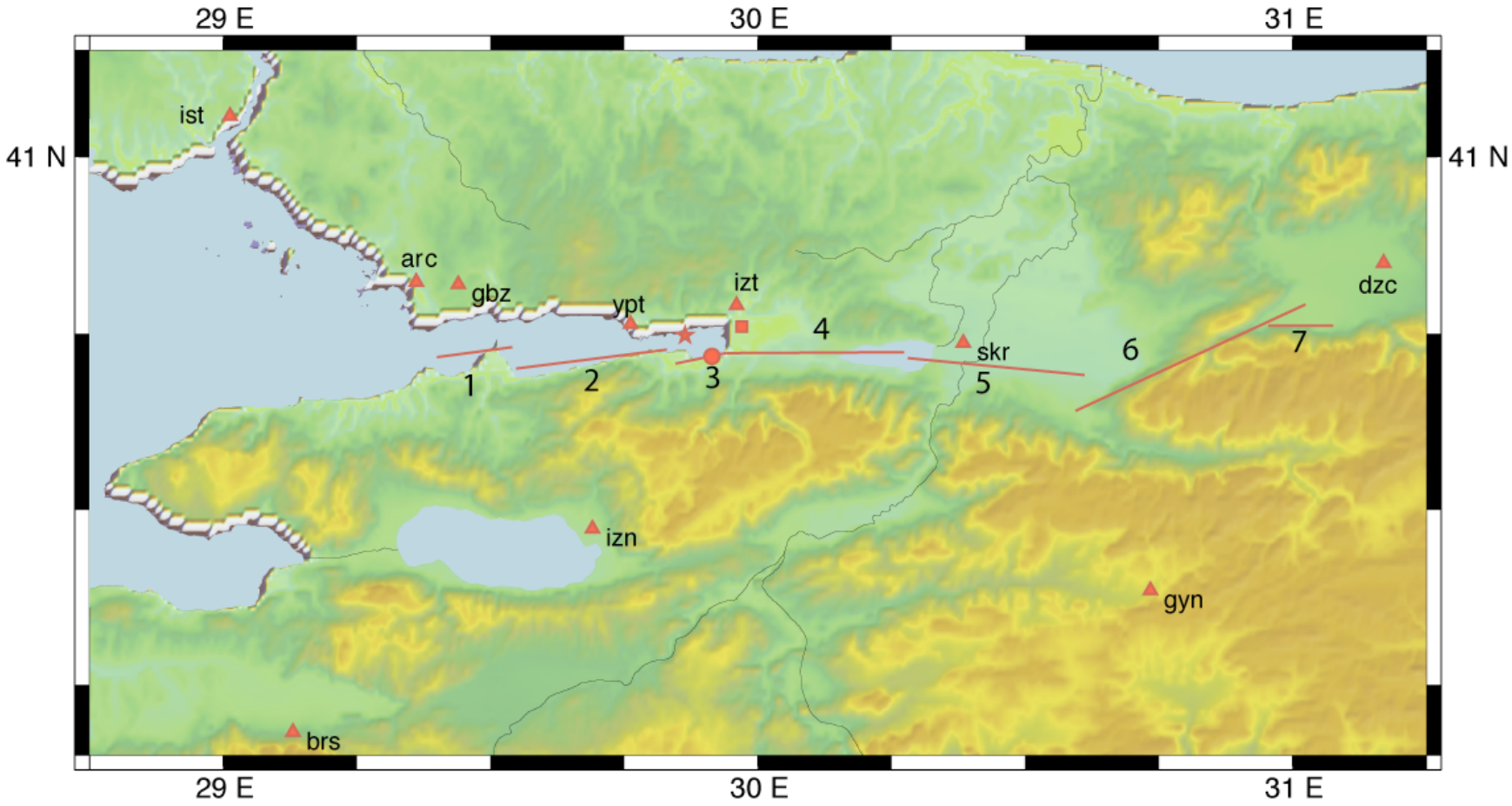

Figure 20. Map of the fault rupture segments (red lines) and strong motion recording stations (red triangles) of the 1999 Kocaeli earthquake. Source: Thio (2005).

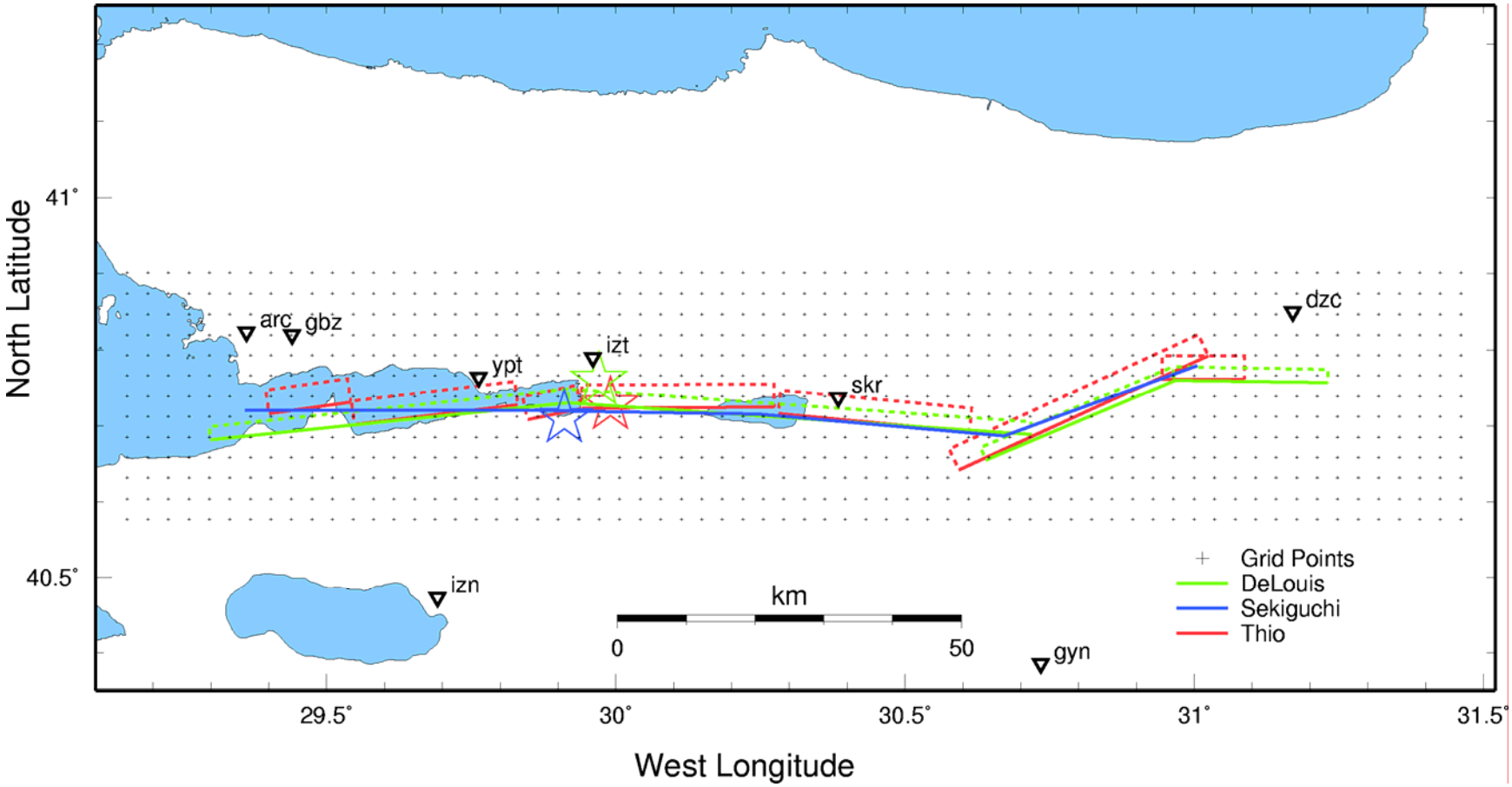

Figure 21. Fault model locations, recording station locations, and ground motion simulation grid locations for the 1999 Izmit earthquake.

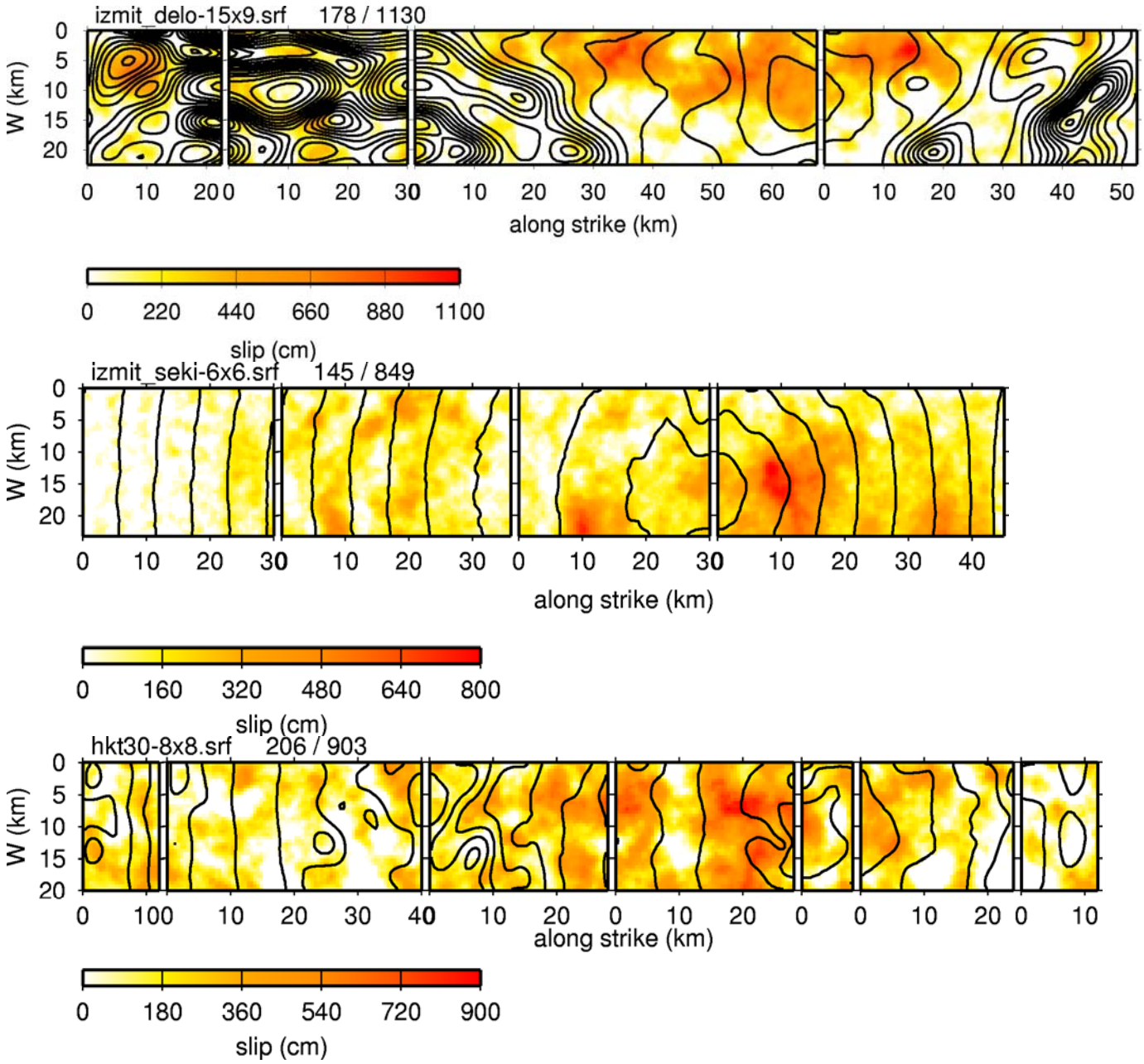

Figure 22. Rupture models (slip and contoured rupture time) of the 1999 Izmit earthquake from (top to bottom) Delouis, Sekiguchi, and Thio.

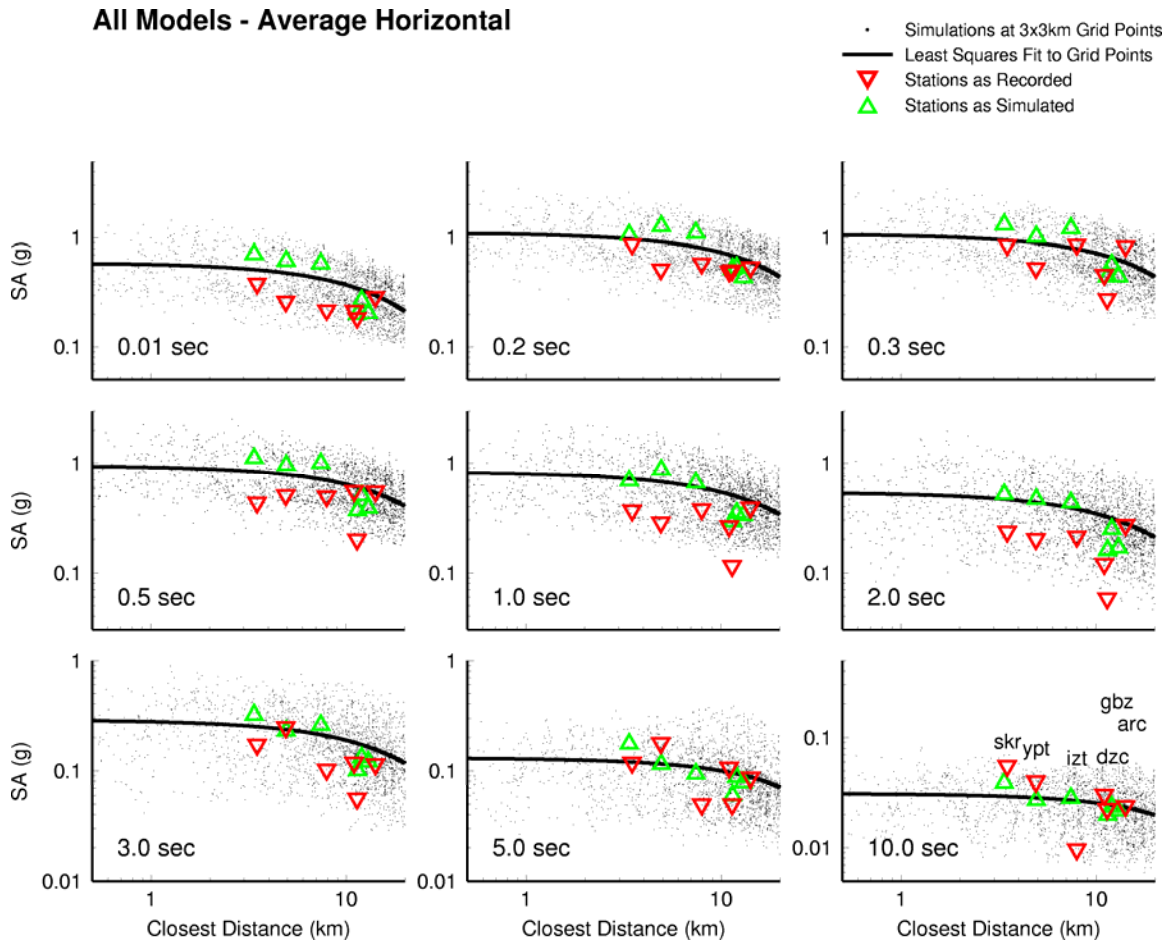

Figure 23. Averaged recorded and simulated ground motions for the three rupture models of the 1999 Izmit earthquake.

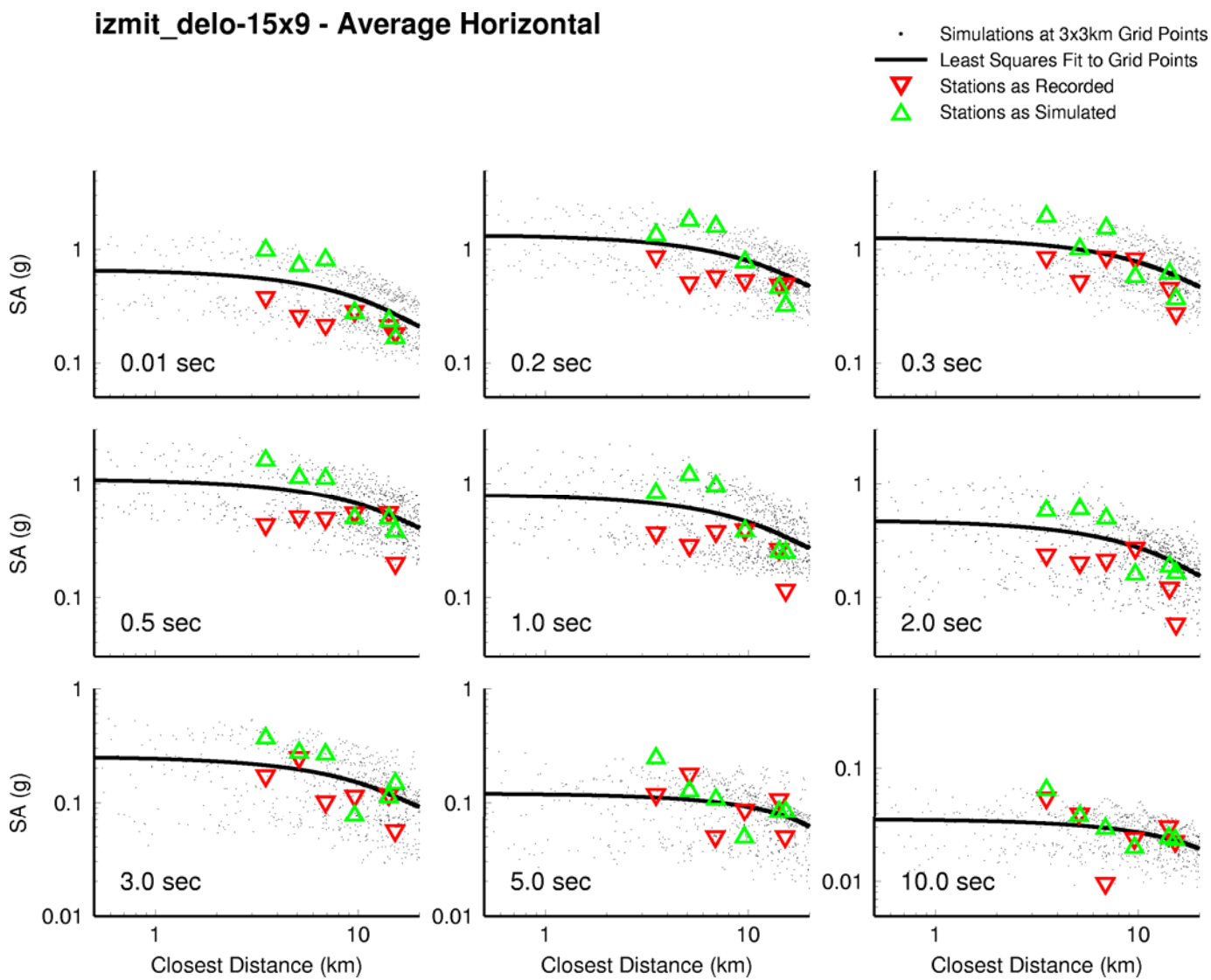

Figure 24. Recorded and simulated ground motions for the Delouis et al. (2002) rupture model of the 1999 Izmit earthquake.

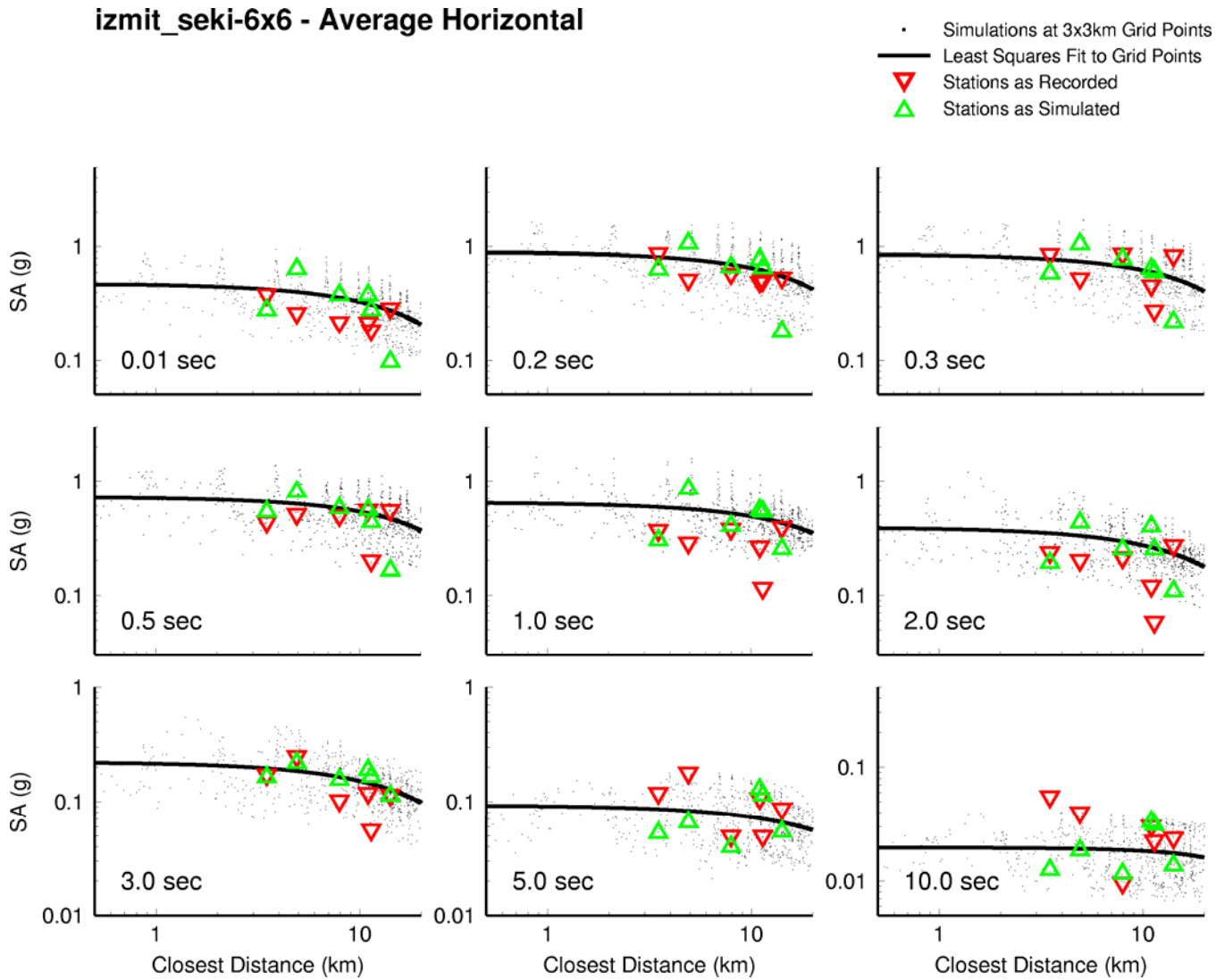

Figure 25. Recorded and simulated ground motions for the Sekiguchi et al. (2002) rupture model of the 1999 Izmit earthquake.

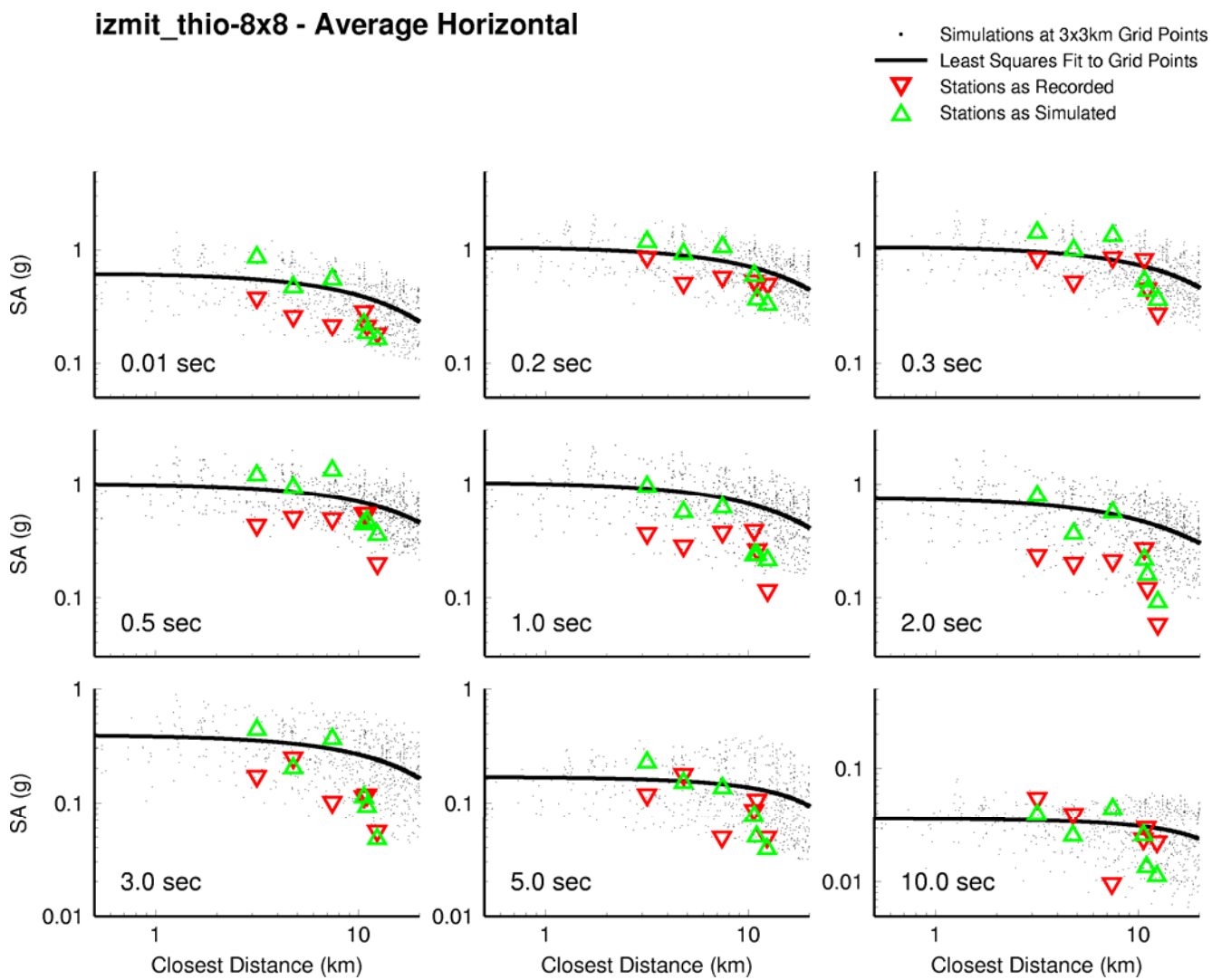

Figure 26. Recorded and simulated ground motions for the Thio al. (2005) rupture model of the 1999 Izmit earthquake.

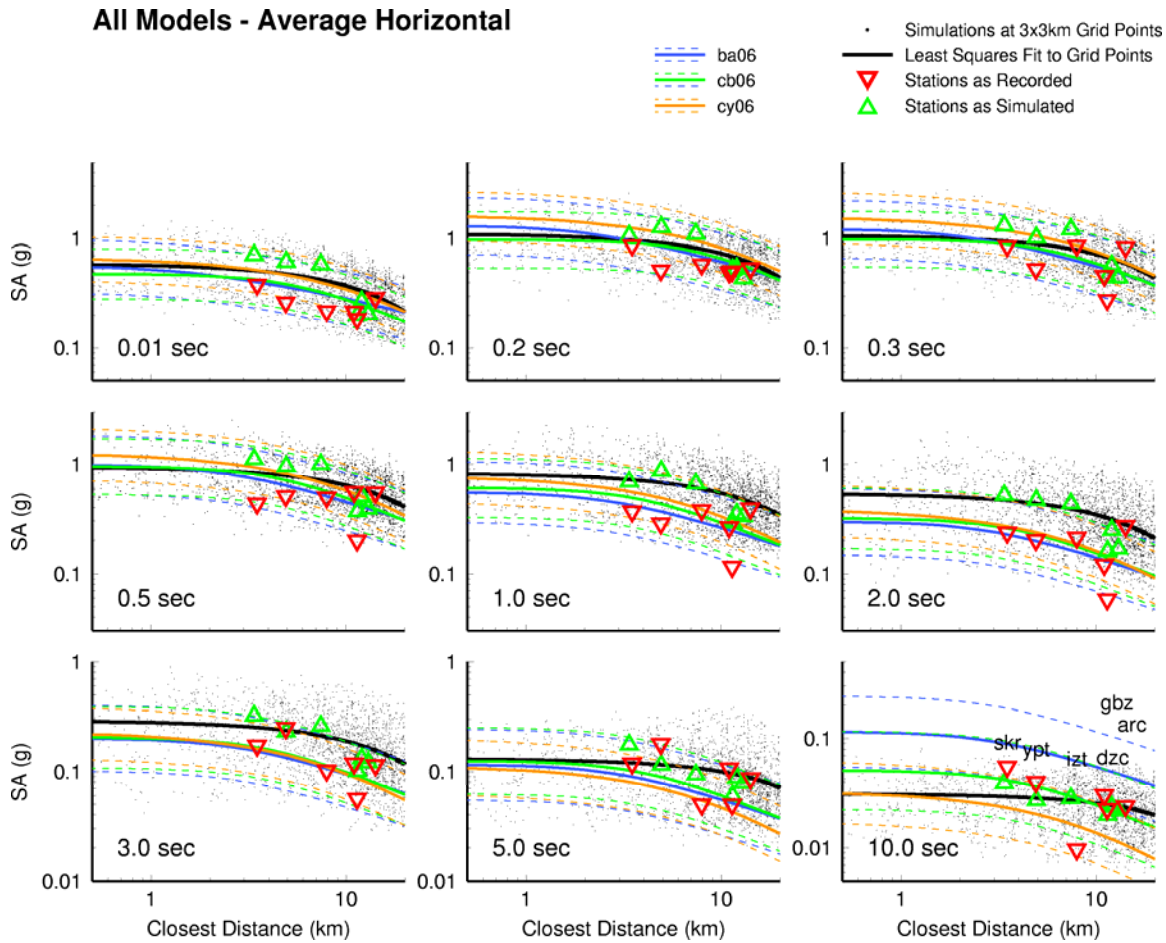

Figure 27. Averaged recorded, simulated and NGA ground motions for the three rupture models of the 1999 Izmit earthquake.

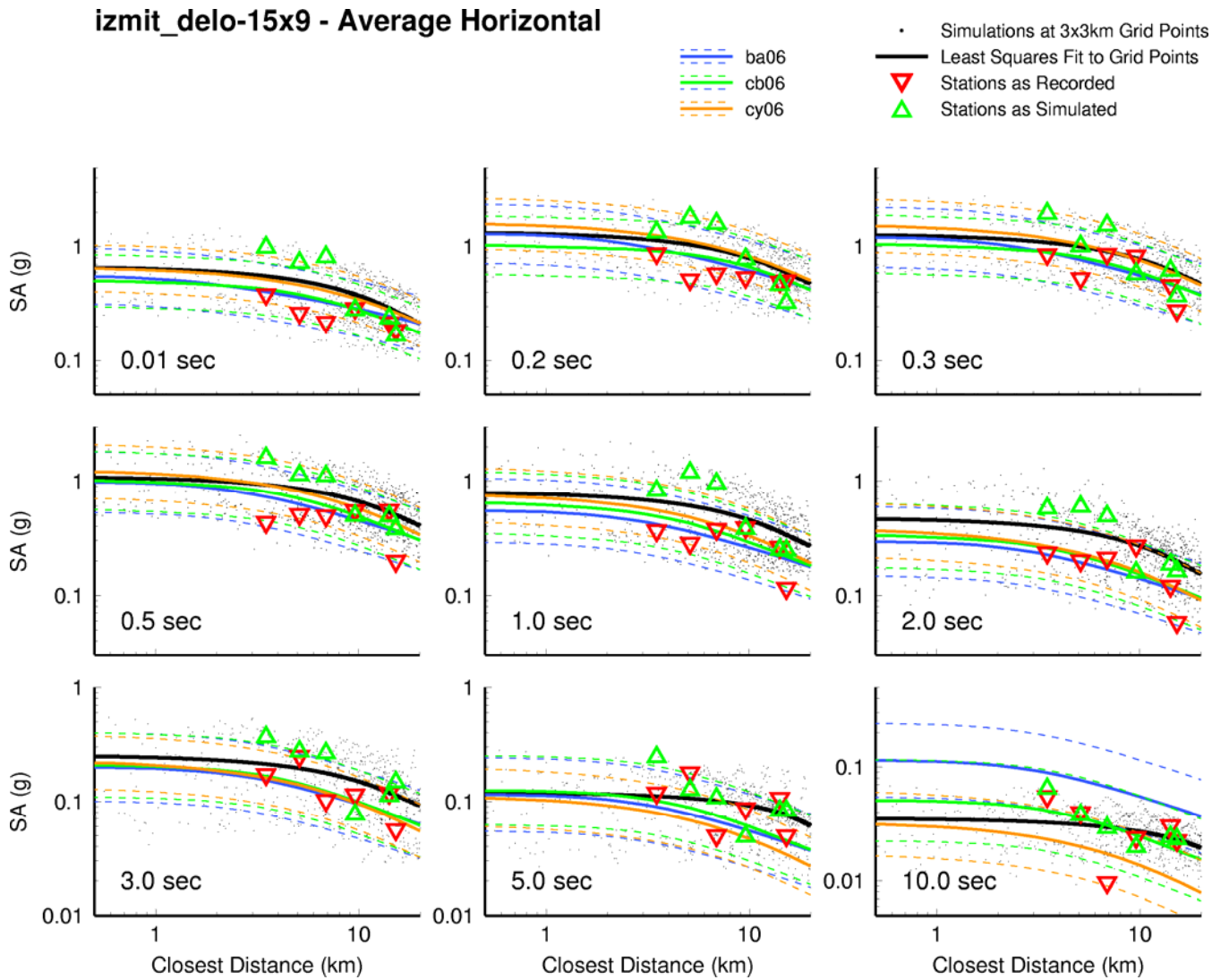

Figure 28. Recorded, simulated and NGA ground motions for the Delouis et al. (2002) rupture model of the 1999 Izmit earthquake.

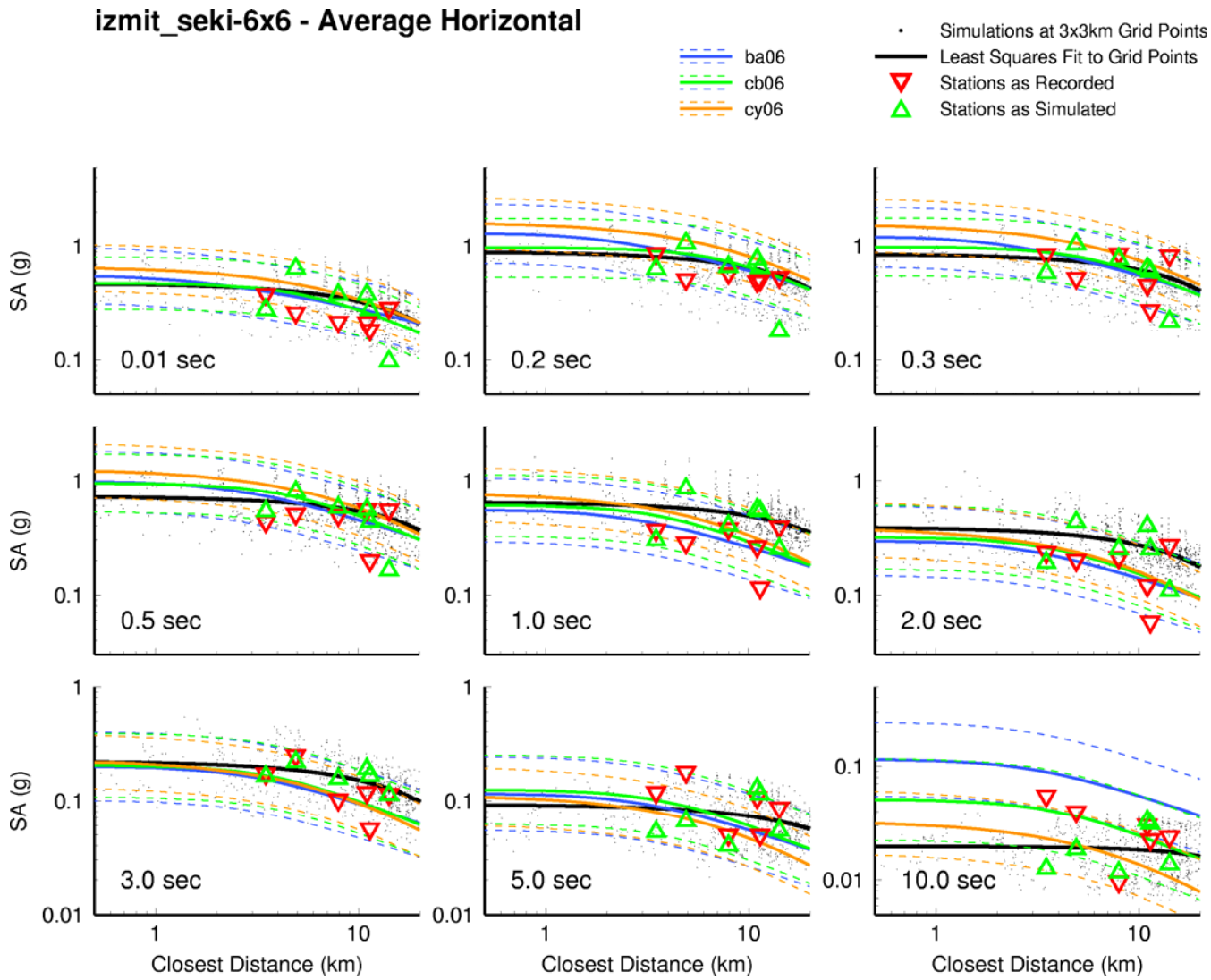

Figure 29. Recorded, simulated and NGA ground motions for the Sekiguchi et al. (2002) rupture model of the 1999 Izmit earthquake.

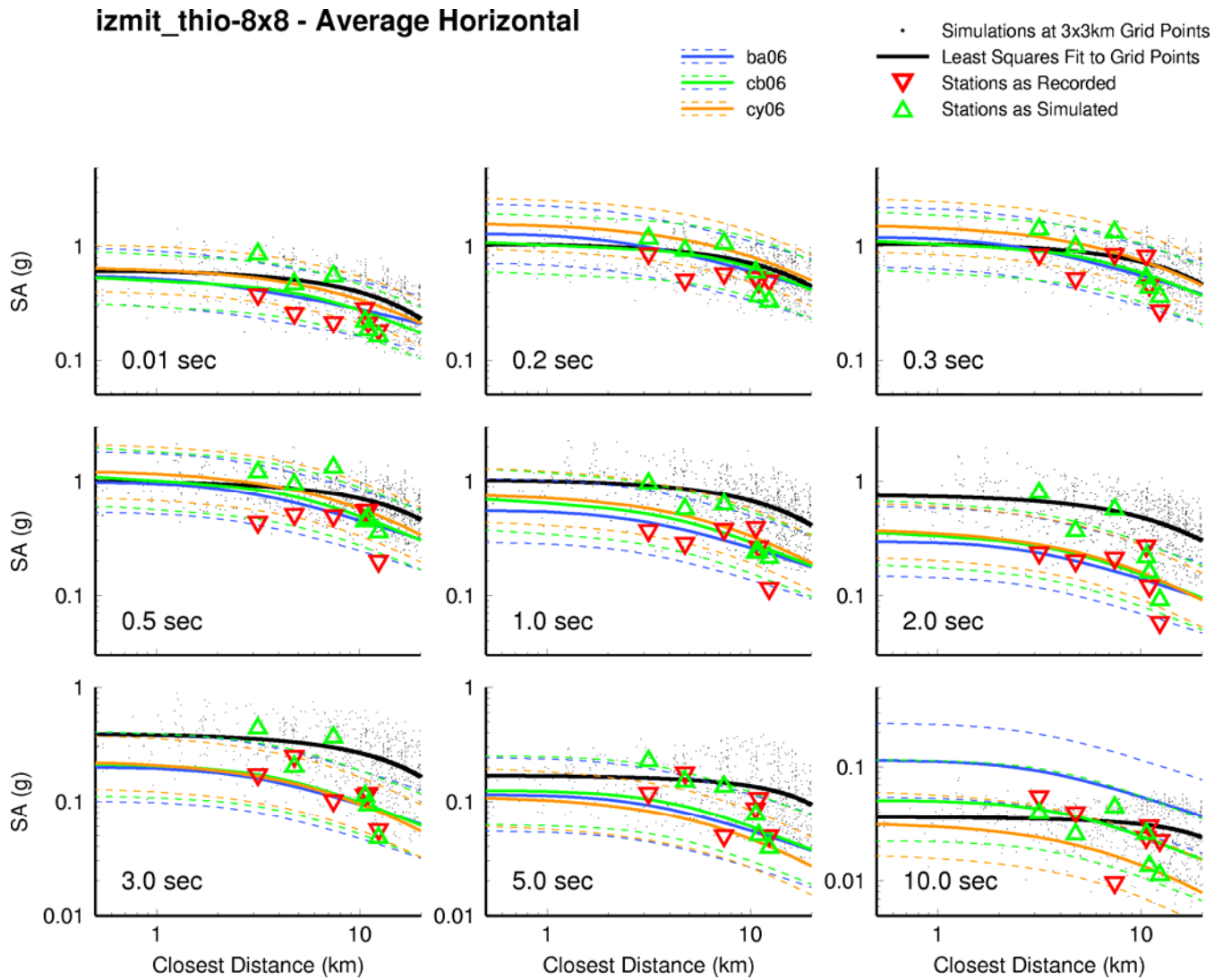

Figure 30. Recorded, simulated and NGA ground motions for the Thio et al. (2002) rupture model of the 1999 Izmit earthquake.

APPENDIX

CURRENT STATE OF KNOWLEDGE ABOUT GROUND MOTIONS FROM LARGE CRUSTAL EARTHQUAKES

We have investigated several physical phenomena that might give rise to the observations of weak ground motions from large shallow earthquakes. In the following, we describe these observations in some detail, and summarize potential explanations of these observations, which include supersonic rupture velocity, the magnitude scaling of the rupture directivity pulse, and rupture dynamics in a crustal model containing a weak shallow layer. We then describe a kinematic broadband ground motion simulation method whose source representation is based on constraints from rupture dynamics, and show that it can model the observed differences in ground motion characteristics between surface and buried faulting in a set of five earthquakes that includes the 1999 Kocaeli earthquake.

Differences Between Shallow and Buried Faulting Earthquakes

Most earthquakes do not break the ground surface unless they achieve magnitudes in the range of 6.5 to 7 or larger. At short and intermediate periods (0.3-3.0s) the recorded ground motions from earthquakes that produce large surface rupture are systematically weaker than the ground motions from earthquakes whose rupture is confined to the subsurface. Somerville (2003) and Kagawa et al. (2004) have shown that earthquakes with surface rupture have asperities (regions of large slip, as defined by Somerville et al., 1999) at depths shallower than 5 km (and possibly others that are deeper), while earthquakes with subsurface rupture have asperities that are all deeper than 5 km.

The large differences in ground motion levels between surface and buried faulting events are evident in Figure A1, which shows the response spectra of near-fault recordings of recent large earthquakes. The left panel shows recordings from four surface faulting earthquakes in the M_w range of 7.4 to 7.9, and the right panel shows recordings from two buried faulting earthquakes of magnitude M_w 6.7 and 7.0. The response spectra of the buried faulting earthquakes are much stronger than those of the larger shallow earthquakes for periods less than 1.5 sec. Figure A2 shows the event terms for larger sets of surface rupture earthquakes at the top, and subsurface rupture earthquakes at the bottom. The unit line represents the Abrahamson and Silva (1977) model, and lines above this line indicate that the event's ground motions on average exceed the model (Abrahamson et al., 1990). The ground motions of the subsurface rupture earthquakes are systematically stronger than average, and those of the surface rupture earthquakes are weaker that average, over a broad period range centered at one second. This phenomenon is not region dependent, since the data are from crustal earthquakes in different tectonically active regions around the world (Kagawa et al., 2004).

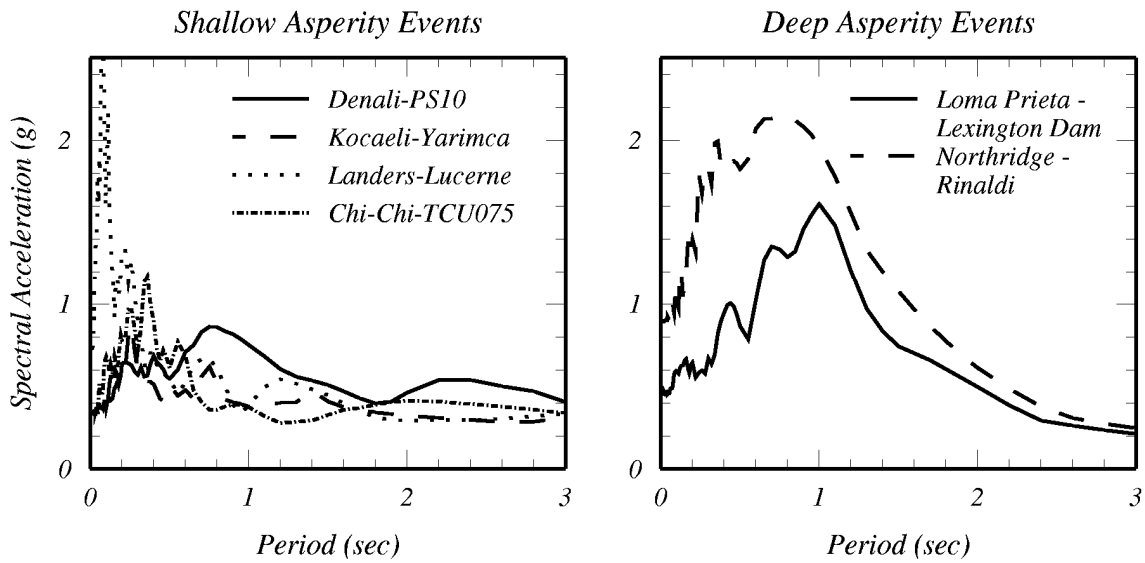

Figure A1. Near-fault response spectra of recent large earthquakes. Left: Four earthquakes, Mw 7.2 to 7.9, with shallow asperities and large surface faulting. Right: Two earthquakes, Mw 6.7 and 7.0, with deep asperities and no surface faulting. Source: Somerville (2003).

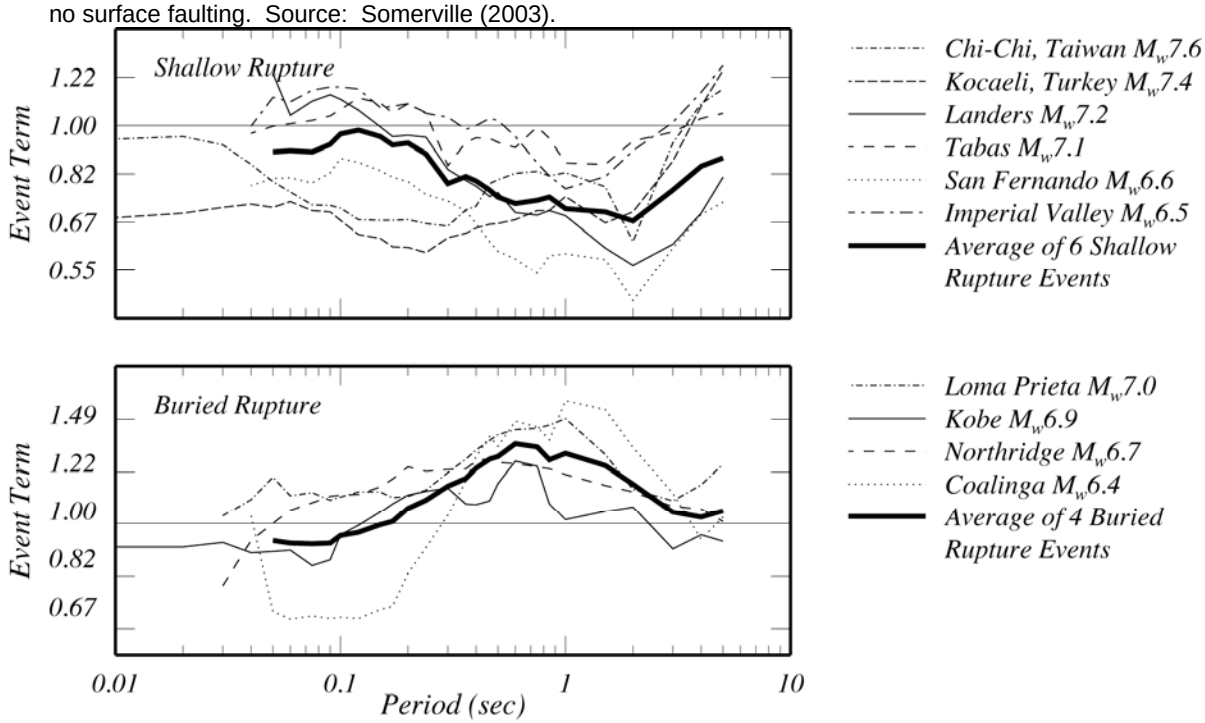

Figure A2. Comparison of response spectral amplitude of individual earthquakes having surface rupture (top) and buried rupture (bottom), averaged over recording sites, with the amplitude of the average earthquake as represented by the model of Abrahamson and Silva (1997), represented by the unit line, which accounts for magnitude, closest distance and recording site category. The event terms (residuals) are shown as the ratio of the event to the model. Source: Somerville (2003).

Distribution of Slip and Slip Velocity with Depth

Comparing the distribution of slip with depth, averaged along strike, in the top part of Figure A3, this difference in ground motions between shallow and buried faulting events seems paradoxical because the shallow events have much larger near-surface displacements.

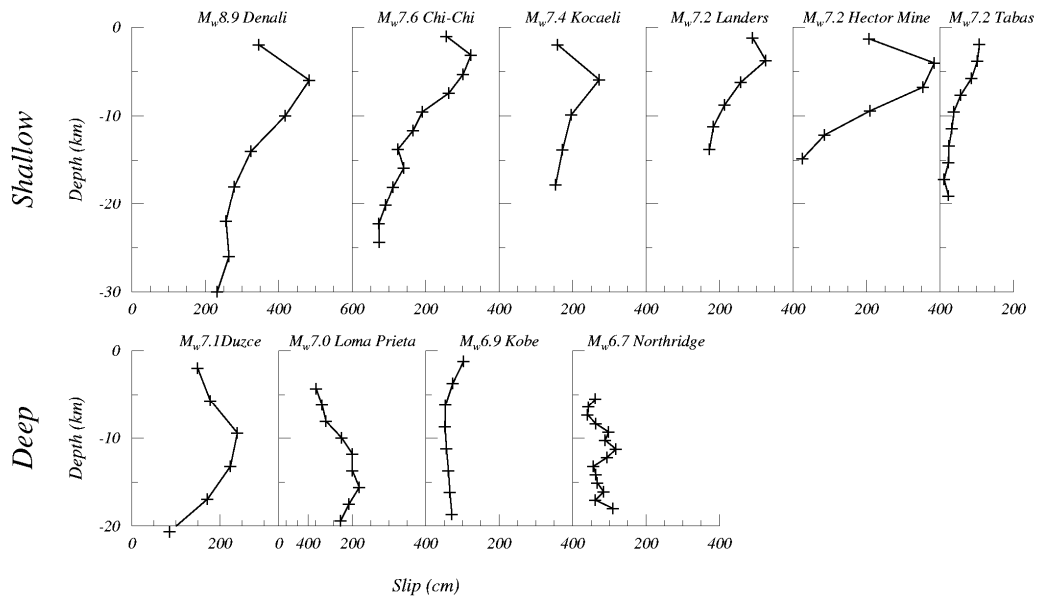

Figure A3. Distribution of slip for shallow (top) and buried faulting (bottom) events. Source: Somerville (2003).

However, slip velocity is a much more important determinant of strong motion levels than fault slip. As shown in Figure A4, the distribution of effective slip velocity with depth for shallow events is quite different from the distribution of slip with depth. (The effective slip velocity is defined by Ishii et al. (2000) as the slip velocity averaged over the time in which the slip grows from 10% to 70% of its final value, and represents the dynamic stress drop). The shallow Kocaeli event has large near-surface displacements, but it does not have correspondingly large slip velocities. The slip velocities of the buried Loma Prieta event are larger than those of the Kocaeli event, causing larger ground motion levels because slip velocity strongly controls strong motion levels. Averaged over 9 shallow events and 8 buried faulting events, the slip velocity of shallow events is about 70% that of buried events. This is true both for the fault as a whole and for the asperities on the fault. We consider that this difference in slip velocity between shallow and buried faulting events is an important aspect of earthquake source characterization for the simulation of strong ground motion.

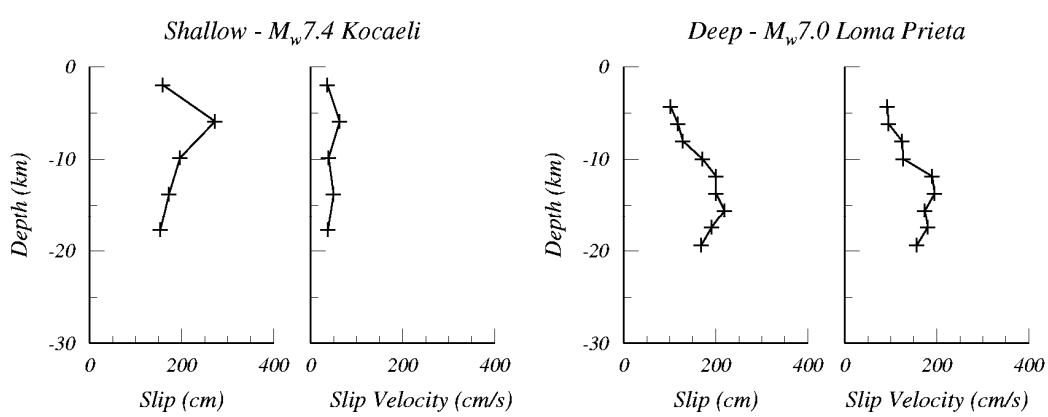

Figure A4. Distribution of slip (left panel) and slip velocity (right panel) for the shallow Kocaeli (left) and buried faulting Loma Prieta (right) earthquakes. Source: Somerville (2003).

Insights from Dynamic Rupture Models of Past Earthquakes

We are involved in international collaboration with Japanese researchers for the systematic analysis of dynamic rupture models of crustal earthquakes (Pitarka, 2005; Mai et al., 2005). The fracture energy is found to be large for surface faulting events, and small for subsurface faults, as shown in Figure A5, in which the events on the left side are for surface faulting, and the events on the right side are for buried faulting. The large fracture energy of shallow events reduces the amount of energy available for seismic radiation, causing such events to produce mainly long period seismic radiation. This is consistent with surface faulting events producing weak high frequency ground motions as described in Figures A1 and A2. Abercrombie and Rice (2005) and Tinti et al. (2005) both show that fracture energy increases with seismic moment. This would cause a corresponding decrease in radiated energy, inhibiting the growth of strong motion amplitudes with increasing seismic moment for earthquakes that are large enough to break the surface, and thus tending to limit the growth of ground motion amplitudes with magnitude.

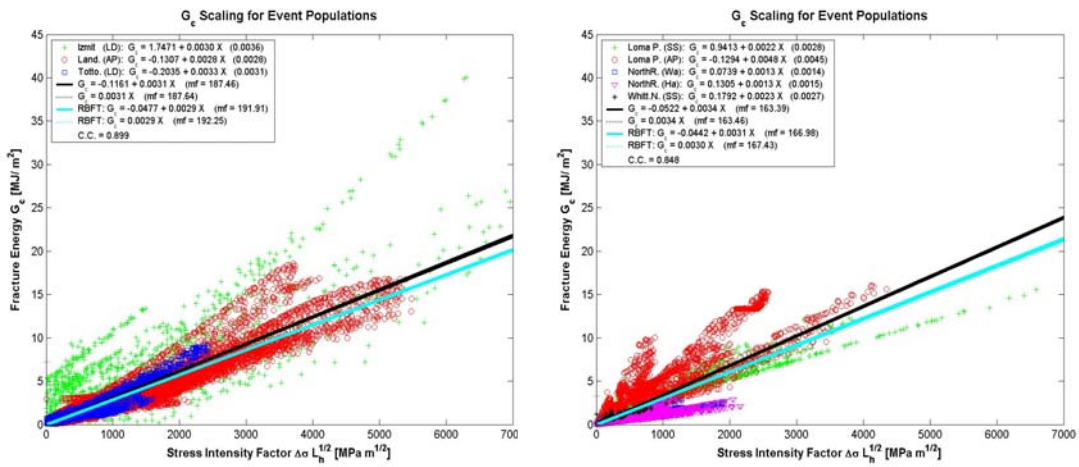

Figure A5. Distribution of fracture energy (vertical axis) and stress intensity factor (horizontal axis) for surface rupture (left) and buried rupture (right) events. Source: Mai et al. (2005).

Both numerical models (Day and Ely, 2002) and laboratory models (Brune and Anooshehpoor, 1988) of the weak zone have revealed its significant effects on rupture dynamics and near-fault particle motion. In the weak zone, the friction increases with sliding velocity (velocity strengthening), and the dynamic friction is quite low compared with that in the deeper part of the fault. Velocity strengthening causes negative or small positive stress drop, and reduces the radiated seismic energy. Consequently, the contribution to the ground motion from shallow asperities is low. Rock mechanics experiments have shown that the presence of a thick gouge layer produces similar effects (e.g. Marone and Scholz, 1988; Shimamoto and Logan, 1981). We expect that the effect of velocity strengthening is significant for shallow slip on existing faults and in soft sedimentary rocks.

Estimates of the slip weakening distance Dc from dynamic rupture models have been summarized by Mai et al. (2005). It is notable that the 1994 Northridge earthquake had an unusually short slip weakening distance, between 0.1 and 0.15 meters, as estimated by three separate studies (Nielsen and Olsen, 2000; Oglesby and Day, 2002; and Hartzell et al., 2005), in contrast with values of 0.4 to 0.9m, 0.4 – 1.5m, and 0.8 – 3.5 m for the Tottori, Kobe and Landers earthquakes respectively. Among the four events analyzed, the Northridge earthquake is the only thrust event, and the only event having no surface rupture. These measurements of fracture energy and slip weakening distance are consistent with rupture in the shallow part of the fault (upper 5 km) being controlled by velocity strengthening, with larger slip weakening distance Dc, larger fracture energy, larger energy absorption from the crack tip, lower rupture velocity, and lower slip velocity than at greater depths on the fault, resulting in lower ground motions for surface faulting than for buried faulting events.

Dynamic Rupture Modeling of Surface and Buried Faulting

We have used rupture dynamic modeling to shed light on the physics of why surface faulting earthquakes have weaker ground motions than those of buried faulting (Somerville and Pitarka, 2006). The top panel of Figure A6 is a buried rupture, and the panels below it are for surface rupture with increasingly weak shallow zones (represented by decreasing values of stress drop) in the upper 5 km of the crust. With increasing weakness, the shallow zone is increasingly effective at arresting the upward propagation of rupture to the surface, reducing the slip velocity on the fault, and reducing the strength of the ground motion. The ratio of buried to surface spectral acceleration is shown as a function of frequency in the third column of Figure A6. For increasingly low values of strength of the shallow zone, the ground motion values become increasingly weak. The right hand column of Figure A6 shows much larger slip velocities on the fault for the buried rupture case than for the surface faulting cases having weak shallow layers. This shows that we can find realistic rheological models of the shallow part of the fault that are consistent with the observation of weaker ground motions from surface faulting earthquakes.

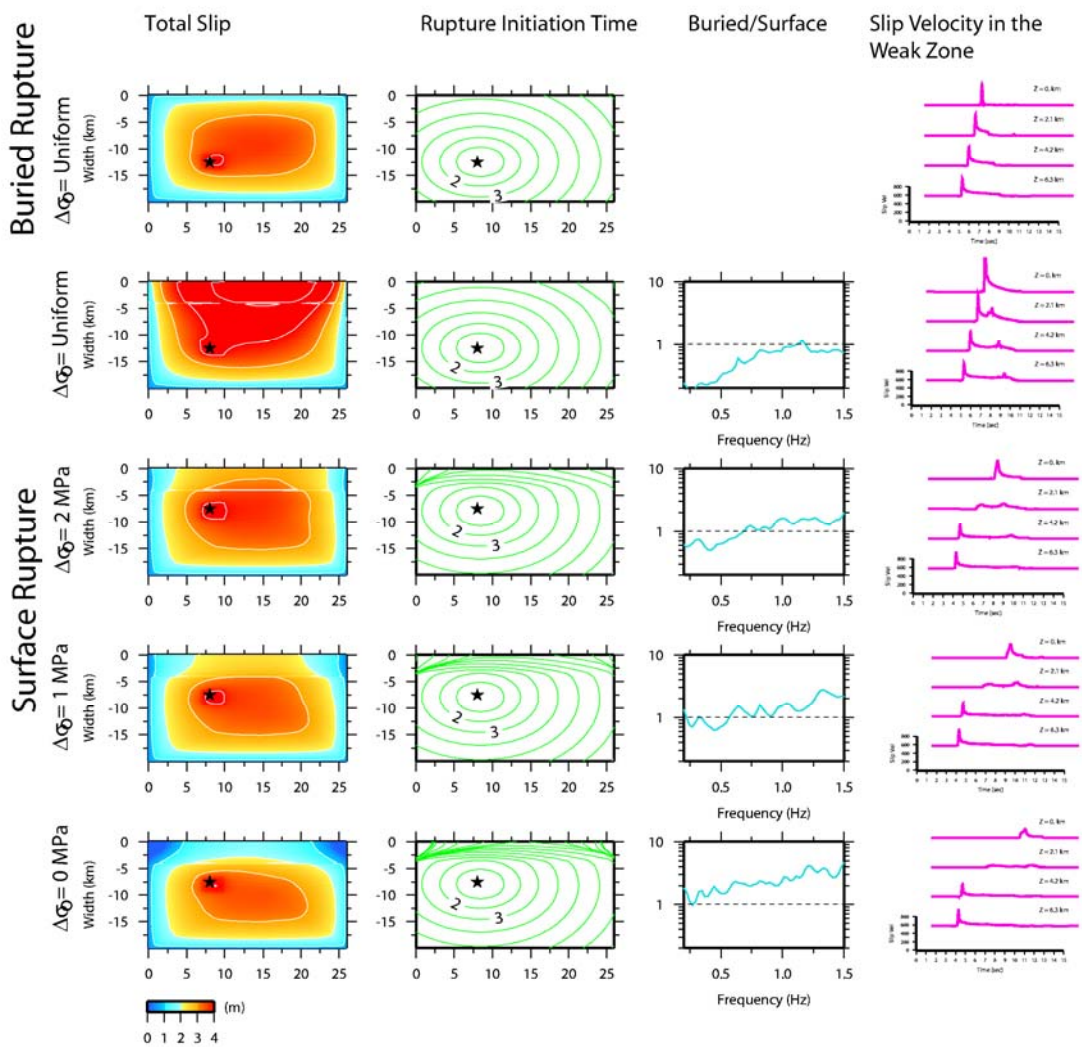

Figure A6. Dynamic simulation of buried and surface rupture earthquakes. The top panel is a buried rupture, and the panels below it are for surface rupture with increasingly weak shallow zones in the upper 5 km of the crust. The shallow zone is increasingly effective at arresting the upward propagation of rupture to the surface, reducing the slip velocity on the fault, and reducing the strength of the ground motion. Source: Somerville and Pitarka (2006).

Magnitude Scaling of the Rupture Directivity Pulse

Somerville (2003) described the magnitude dependence of the near fault rupture directivity pulse. The rupture directivity pulses of earthquakes in the magnitude range of 6.7 to 7 have much shorter periods than the pulses from earthquakes in the magnitude range of 7.2 to 7.6 (left side of Figure A7). The narrow band nature of these pulses causes their elastic response spectra to have peaks. The fault-normal components of the response spectra (which contain the directivity pulse) are shown as solid red lines, and the fault-parallel components, which as expected are much smaller at long periods, are shown by long dashed blue lines on the right side of Figure A7. The 1994 UBC spectrum for soil site conditions is used as a reference model for comparison. The fault-normal spectra for the large earthquakes (right column) are compatible with the UBC code spectrum in the intermediate period range, between 0.5 and 2.5 seconds, but have a bump at a period of about 4 seconds where they significantly exceed the UBC code spectrum. In contrast, the fault-normal spectra of the smaller earthquakes (left column) are much larger than the UBC code spectrum for periods of 0.5 - 2.5 sec, but are similar to the UBC spectrum at longer periods. Figure A7 also reflects the differences between surface and buried faulting described above.

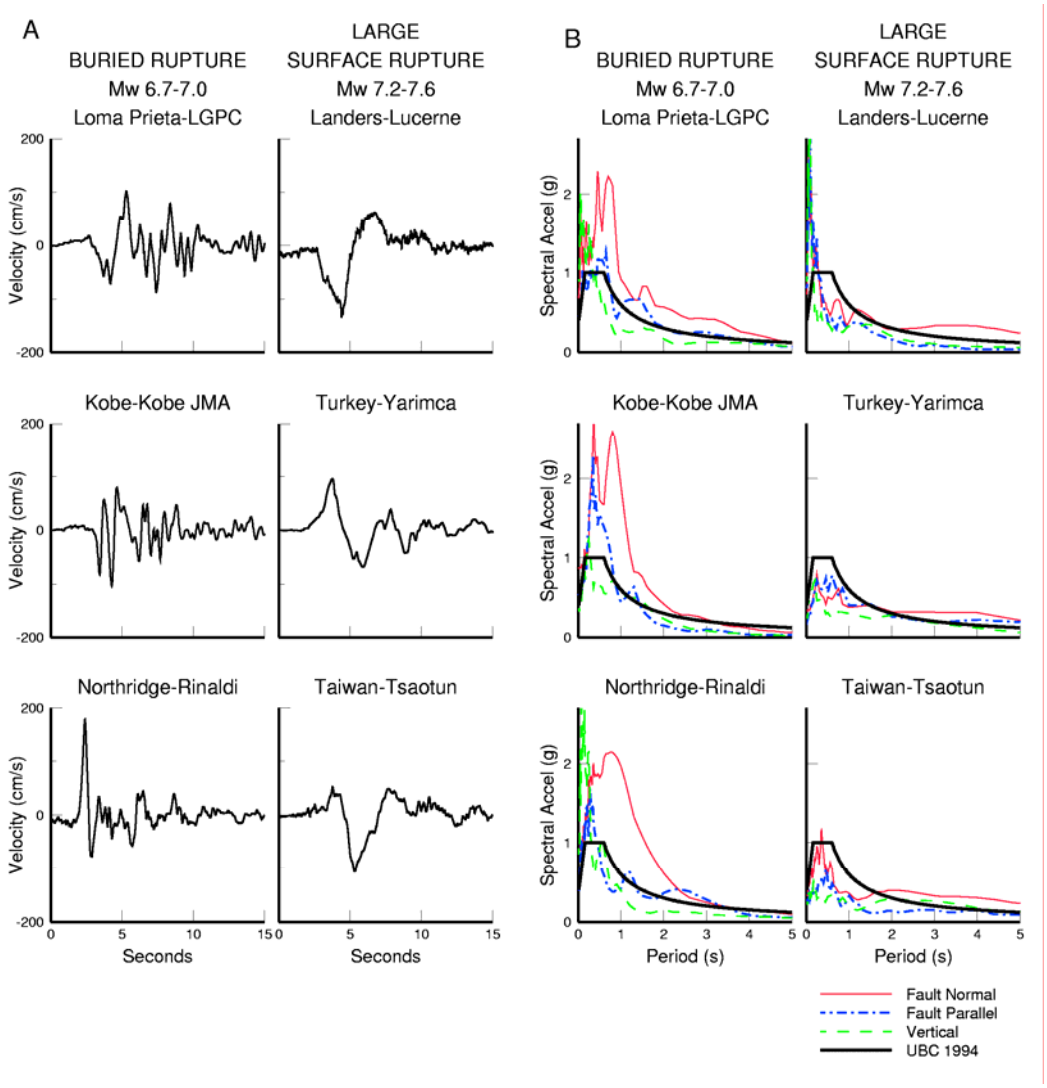

Figure A7. A: Fault-normal velocity pulses recorded near three moderate magnitude earthquakes (left column) and three large earthquakes (right column), shown on the same scales. B: Corresponding acceleration response spectra, with the 1994 UBC code spectrum shown for comparison. Source: Somerville (2003).

Figure A7 suggests that the near-fault response spectra of smaller earthquakes may be stronger than the response spectra of larger earthquakes in some period ranges. Peak velocity increases strongly with magnitude at small and intermediate magnitudes, but for larger earthquakes there may be saturation of near fault peak velocity with magnitude related to the magnitude dependence of the period of the directivity pulse.

Rupture Velocity

We have just shown that the strongest ground motions at near fault sites are controlled by rupture directivity effects (Somerville et al., 1997). Subshear rupture causes the buildup of coherent energy in the forward rupture direction. This directivity effect increases as the rupture velocity approaches the shear wave velocity, and may be dissipated when the rupture velocity becomes supershear. There is evidence for rupture velocities exceeding the shear wave velocity in both the 1999 Kocaeli, Turkey earthquake (Anderson, 2000; Bouchon et al., 2000; 2001, Sekiguchi and Iwata, 2002; Thio et al., 2005) and the 2002 Denali, Alaska earthquake (Ellsworth et al., 2004; Aagaard and Heaton, 2004; Dunham and Archuleta, 2005). There is ambiguity in the interpretation of the Sakarya recording of the Kocaeli earthquake, whose fault normal component was not functional and whose triggering has been questioned by some investigators. The PS10 recording 3 km from the 2002 Denali fault has ground velocity waveforms that are very different from those typical of rupture directivity, and it is likely that this recording was influenced by rupture velocities larger than the shear wave velocity.

Aagaard et al. (2004) show that the effect of rupture velocity larger than the shear wave velocity is to reduce the level of the long period ground motion. For short periods, Spudich (2006) uses isochrone theory to argue that the short period content of S pulses from supershear rupture depends on the balance of source-related diminution and propagation-related enrichment. Simulated ground motion levels are strongly dependent on the rupture velocities of the rupture models that are used. Accordingly, we used several rupture models for each earthquake, each with different representations of their rupture velocities, to perform simulations of the recorded ground motions. From these results, we will assess which rupture models are most compatible with the recorded ground motions, and evaluate the role of supershear rupture velocity in potentially reducing the level of the recorded ground motions. Based on these comparisons with recorded data, we will be in a position to use large scale simulations to assess the effect of rupture velocity on the level of ground motions along the entire lengths of the Kocaeli and Denali ruptures.

REFERENCES

Aagaard, B. and T. Heaton (2004). Near-source ground motions from simulations of sustained intersonic and supersonic fault ruptures. *Bull. Seism. Soc. Am* 94, 2064-2078.

Abercrombie, R.E, and J.R. Rice, Can observations of earthquake scaling constrain slip-weakening? *Geophys. J. Int.,* (in press), 2005.

Abrahamson, N. (2006). Abrahamson-Silva NGA Model, *Proceedings of the Eighth National Conference on Earthquake Engineering*, San Francisco, California.

Abrahamson, N.A., P.G. Somerville, and C. Allin Cornell (1990). Uncertainty in numerical strong motion predictions, *Proc. 4th U.S. National Conference on Earthquake Engineering*, **1**, 407- 416.

Abrahamson, N.A. and W.J. Silva (1997). Empirical response spectral attenuation relations for shallow crustal earthquakes. Seism. Res. Lett. 68, 94-127.

Abrahamson, N.A. and K.M. Shedlock (1997). Overview (of attenuation relations). Seism. Res. Lett. 68, 9-23.

Anderson, J.G. (2000). Implications for seismic hazard analysis, in *Kocaeli, Turkey, Earthquake of August 17, 1999: Reconnaissance Report*. Earthquake Spectra 16, 113-117.

Asano, K., T. Iwata and K. Irikura (2005). Estimation of source rupture process and strong ground motion simulation of the 2002 Denali, Alaska, earthquake. *Bull. Seism. Soc. Am*. 95, 1701-1715.

Atkinson, G. (2006). Boore-Atkinson NGA Model, *Proceedings of the Eighth National Conference on Earthquake Engineering*, San Francisco, California.

Bouchon, M., N. Toksoz, H. Karabulut, M.P. Bouin, M. Dietrich, M. Aktar, and M. Edie (2000). Seismic imaging of the 1999 Izmit (Turkey) rupture inferred from the near-fault recordings. *Geophysical Research Letters* 27, 3013-3016.

Bouchon, M., M.P. Bouin, H. Karabulut, M.N. Toksoz, M. Dietrich, and A.J. Rosakis (2001). How fast is rupture during an earthquake? New insights from the 1999 Turkey earthquakes. *Geophysical Research Letters* 28, 2723-2726.

Brune, J.N. and R. Anooshehpoor (1988). A physical model of the effect of a shallow weak layer on strong ground motion for strike-slip ruptures. *Bull. Seism. Soc. Am* .88, 1070-1078.

Campbell, K. and Y. Bozorgnia (2006). Campbell-Bozorgnia Next Generation Attenuation (NGA) Relations for PGA, PGV and Spectral Acceleration: A Progress Report, *Proceedings of the Eighth National Conference on Earthquake Engineering*, San Francisco, California.

Chiou, B. and R. Youngs (2006). PEER-NGA Empirical Ground Motion Model for Horizontal Spectral Accelerations from Earthquakes in Active Tectonic Regions, *Proceedings of the Eighth National Conference on Earthquake Engineering*, San Francisco, California.

Day, S.M, and G.P. Ely (2002). Effect of a shallow weak zone on fault rupture: numerical simulation of scale-model experiments. *Bull. Seism. Soc. Am* 92, 3022-3041.

Delouis, B., D. Giardini, P. Lundgren, and J. Salichon (2002). Joint inversion of InSAR, GPS, teleseismic, and strong-motion data for the spatial and temporal distribution of earthquake slip: Application to the 1999 Izmit mainshock, *Bulletin of the Seismological Society of America, 92* (1), 278-299.

Dreger, D.S., D. Oglesby, R. Harris, N. Ratchkovski, and R. Hansen (2004). Kinematic and dynamic models of the November 3, 2002 Mw 7.9 Denali, Alaska earthquake. Geophys. Res. Lett. 31, L04605.

Dunham, E.M., and R.J. Archuleta (2004). Evidence for a supershear transient during the 2002 Denali earthquake. *Bull. Seism. Soc. Am.,* in press.

Ellsworth, W.L. et al. (2004). Near-field ground motion of the 2002 Denali fault, Alaska, earthquake recorded at Pump Station 10. Earthquake Spectra 20, 597-615.

Frankel, A. (2006). Scaling of high frequency ground motions for the Sumatra, Chi-chi, and Kocaeli earthquake sequences. *Proceedings of the Eighth National Conference on Earthquake Engineering,* San Francisco, CA.

Graves, R.W. and A. Pitarka (2004). Broadband time history simulation using a hybrid approach. *Proceedings of the 13th World Conference on Earthquake Engineering*, Vancouver, Canada, August 1-6, 2004, Paper No. 1098.

Guatteri, M., P.M. Mai, G.C. Beroza, and J. Boatwright (2003). Strong ground motion prediction from stochastic – dynamic source models. *Bull. Seism. Soc. Am* 93, 301-313.

Haeussler, P.J. and F. Naeim (editors) (2004). 2002 Denali fault, Alaska earthquake reconnaissance report. Earthquake Spectra 20, 555-738.

Hartzell, S.H., M. Guatteri, P.M. Mai, P.-C. Liu, and M. Fisk (2005). Calculation of broadband time histories of ground motion, Part II: Kinematic and dynamic modeling using theoretical Green's functions and comparison with the 1994 Northridge earthquake. Unpublished manuscript.

Hisada, Y. (2001). A theoretical omega-square model considering spatial variation in slip and rupture velocity. *Bull. Seism. Soc. Am*. 91, 651-666.

Idriss, I.M. (2006). Idriss NGA Model, *Proceedings of the Eighth National Conference on Earthquake Engineering*, San Francisco, California.

Ishii, T., T. Sato and Paul G. Somerville (2000). Identification of main rupture areas of heterogeneous fault models for strong motion estimation. *J. Struct. Constr. Eng., AIJ*, No. 527, 61-70.

Kagawa, T., K. Irikura and P. Somerville (2004). Differences in ground motion and fault rupture process between the surface and buried rupture earthquakes. *Earth, Planets and Space* 56, 3-14.

Mai, P.M., P. Somerville, A. Pitarka, L. Dalguer, H. Miyake, S. Song, G. Beroza, and K. Irikura (2005). On the scaling of dynamic source parameters and their relation to near-source ground motion prediction. *Seismological Research Letters* 76, p.261.

Marone, C. and C. Scholtz (1988). The depth of seismic faulting and the upper transition from stable to unstable slip regimes, *Geophys. Res. Lett*. 15,621-624.

Neilsen, S. and K.B. Olsen (2000). Constraints on stress and friction from dynamic rupture models of the 1994 Northridge, California earthquake. *Pure App. Geophys*. 157, 2029-2046.

Oglesby, D.D., D.S. Dreger, R.A. Harris, N. Ratchkovski, and R. Hansen (2004). Inverse kinematic and forward dynamic models of the 2002 Denali, Alaska earthquake. Bull. Seism. Soc. Am. 94, S214-S233.

Oglesby, D.D. and S.M. Day (2002). Stochastic faults: Implications for fault dynamics and ground motion. *Bull. Seism. Soc. Am*. 92, 3006-3021.

Pitarka, A. (2005). Dynamic rupture models of the 1992 Landers and 1989 Loma Prieta earthquakes. Report to Ohsaki Research Institute.

Pitarka, A. and P.G. Somerville (2001). Rapid generation of ground motion maps of the 8/17/99 Turkey and 9/20/99 Taiwan earthquakes. Report to the National Science Foundation.

Scholz, C.H. (2002). The mechanics of earthquakes and faulting. Cambridge University Press, 2nd Edition.

Sekiguchi, H. and T. Iwata (2002). Rupture process of the 1999 Kocaeli, Turkey, earthquake estimated from strong-motion waveforms. *Bull. Seism. Soc. Am*. 92, 300-311.

Shimamoto, T., and J.M. Logan (1981). Effects of simulated clay gouges on the sliding behavior of Tennessee sandstone, Tectonophysics, 75,243-255.

Somerville, P.G. and A. Pitarka (2006). Differences in earthquake source and ground motion characteristics between surface and buried earthquakes. *Proceedings of the Eighth National Conference on Earthquake Engineering*, San Francisco, California.

Somerville, P.G. (2003). Magnitude scaling of the near fault rupture directivity pulse. *Phys. Earth. Planetary. Int*., 137, 201-212.

Somerville, P.G., K. Irikura, R. Graves, S. Sawada, D. Wald, N. Abrahamson, Y. Iwasaki, T. Kagawa, N. Smith and A. Kowada (1999). Characterizing earthquake slip models for the prediction of strong ground motion. *Seismological Research Letters*, 70, 59-80.

Somerville, P.G., N.F. Smith, R.W. Graves, and N.A. Abrahamson (1997). Modification of empirical strong ground motion attenuation relations to include the amplitude and duration effects of rupture directivity, *Seismological Research Letters* 68, 199-222.

Thio, H.K., R.W. Graves, T. Sato, T. Ishii, and P.G. Somerville 2004. A multiple time window rupture model for the 1999 Chi-Chi earthquake from a combined inversion of teleseismic, surface wave, strong motion and GPS data. *J. Geophys. Res.* 109, B08309, doi: 10.1029/2002JB002381.

Thio, H.K., R.W. Graves, J. Polet, T. Sato, T. Ishii, P.G. Somerville, 2005. The source process of the 1999 Kocaeli (Turkey) earthquake, J. *Geophys. Res*., submitted.

Thio, H.K. (2005). The rupture process of the 2002 Alaska earthquake. Geophysical Research Abstracts 5, 13753, European Geophysical Society.

Thio, H.K., R.W. Graves, 2002**.** Rupture process of the 1999 Duzce earthquake, Final report to the PEER Lifelines program.

Tinti, E., P. Spudich, and M. Cocco, Earthquake fracture energy inferred from kinematic rupture models on extended faults, *submitted to J. Geophys. Res*, 2005.

Tsuboi, S., D. Komatitsch, C. Ji, and J. Tromp (2003). Broadband modeling of the 2002 Denali fault earthquake on the Earth Simulator. Phys. Earth Planet Int. 139, 305-312.

Youd, T.L., J.-P. Bardet, and J. D. Bray (editors) (2000). Kocaeli, Turkey earthquake of August 17, 1999 reconnaissance report. Earthquake Spectra 16, Supplement A.